

Desmoglein 2-Dependent Arrhythmogenic Cardiomyopathy Is Caused by a Loss of Adhesive Function

Running title: *Kant et al.; Desmoglein-dependent cardiomyopathy*

Sebastian Kant, MSc¹; Bastian Holthöfer, PhD¹; Thomas M. Magin, PhD²;

Claudia A. Krusche, PhD¹; Rudolf E. Leube, MD¹

¹Institute of Molecular and Cellular Anatomy, RWTH Aachen University, Aachen;

²Institute of Biology and Translational Center for Regenerative Medicine, University of Leipzig,
Leipzig, Germany

Correspondence:

Rudolf Leube, MD

Institute of Molecular and Cellular Anatomy

RWTH Aachen University

Wendlingweg 2

52074 Aachen

Germany

Tel: ++49 241 80 89107

Fax: ++49 241 80 82508

E-mail: rleube@ukaachen.de

Journal Subject Codes: [104] Structure, [130] Animal models of human disease

Abstract:

Background - The desmosomal cadherin desmoglein 2 (Dsg2) localizes to the intercalated disc (ID) coupling adjacent cardiomyocytes. Desmoglein 2 gene (*DSG2*) mutations cause arrhythmogenic cardiomyopathy (AC) in human and transgenic mice. AC is characterized by arrhythmia, cardiomegaly, cardiomyocyte necrosis with replacement fibrosis, interstitial fibrosis and ID dissociation. The genetic *DSG2* constellations encountered are compatible with loss of adhesion and altered signaling. To further elucidate pathomechanisms, we examined whether heart-specific Dsg2 depletion triggers cardiomyopathy.

Methods and Results - Since *DSG2* knock-outs die during early embryogenesis, mice were prepared with cardiomyocyte-specific *DSG2* ablation. Healthy transgenic animals were born with a functional heart presenting IDs with incorporated desmosomal proteins. Dsg2 protein expression was reduced below 3% in the heart. All animals developed AC during postnatal growth with pronounced chamber dilation, calcifying cardiomyocyte necrosis, aseptic inflammation, interstitial and focal replacement fibrosis and conduction defects with altered connexin 43 distribution. Electron microscopy revealed absence of desmosome-like structures and regional loss of ID adhesion. Mice carrying two mutant *DSG2* alleles coding for Dsg2 lacking part of the adhesive EC1-EC2 domains present an indistinguishable phenotype, which is similar to that observed in human AC patients.

Conclusions - The observations show that the presence of Dsg2 is not essential for late heart morphogenesis and for cardiac contractility to support postnatal life. Upon increasing mechanical demands heart function is severely compromised as evidenced by the onset of cardiomyopathy with pronounced morphological alterations. We propose that loss of Dsg2 compromises adhesion and that this is a major pathogenic mechanism in *DSG2*-related and probably other desmosome-related ACs.

Key words: arrhythmogenic right ventricular cardiomyopathy, desmosome, transgenic mice, fibrosis, calcification

Introduction

Arrhythmogenic cardiomyopathy (AC), also referred to as arrhythmogenic right ventricular cardiomyopathy (ARVC) or arrhythmogenic right ventricular dysplasia (ARVD), is a genetic heart disease.¹ It affects primarily the right ventricle, but left ventricular involvement is also quite common. Ventricular tachyarrhythmia, chamber dilation and fibrofatty replacement of cardiac tissue are key features of human AC. During its acute phase, the disease is a frequent cause of sudden cardiac death in young athletes and may lead to heart failure in the chronic phase.

Mutations in desmosomal genes are the most common genetic alterations in AC, which has been referred to as a disease of the desmosome.¹ Mutations in genes encoding phospholamban, desmin, transforming growth factor β 3, transmembrane protein 43 and the ryanodine receptor 2 have also been identified.² Desmosome-like structures are part of the intercalated disc (ID), a composite adhesion site between adjacent cardiomyocytes.³ The ID provides mechanical, electrophysiological and metabolic linkage between neighboring cells. Cardiac desmosomes are specialized multiprotein assemblies consisting of the calcium-dependent cell-cell adhesion transmembrane proteins desmoglein 2 (Dsg2) and desmocollin 2 (Dsc2) and attached linker molecules, i.e. the armadillo repeat-containing plakophilin 2 (Pkp2) and plakoglobin (Pg) and the plakin domain-containing desmoplakin (Dsp), which in turn connects to cytoskeletal desmin intermediate filaments.^{4,5} Although all desmosomal proteins have been implicated in AC, the most commonly mutated genes are those encoding Pkp2 and Dsg2.¹

The observed autosomal dominant inheritance of desmoglein 2 gene (*DSG2*)-related AC cases^{2,6-15} suggests that reduction of the Dsg2 wild type (WT) protein leads to a loss of cardiac

function and/or that Dsg2 mutant (MT) protein exerts a dominant negative effect on the remaining Dsg2 WT protein. Two major types of non-exclusive pathomechanisms have been described to depend on Dsg2. As a cell-cell adhesion molecule it provides adhesive force and thereby supports force transmission between contractile cardiomyocytes. Alternatively, Dsg2 regulates intracellular signaling. This function is expected to be linked to the cytoplasmic domain of Dsg2 and may involve associated signaling molecules such as Pg and Pkp2/PKC α acting through downstream effectors implicating the Wnt and/or Hippo pathways.^{16,17}

To examine mechanisms of *DSG2*-related cardiomyopathy, several murine models have been established. Complete constitutive deletion of Dsg2 was shown to be embryonic lethal¹⁸ as is the case for all other integral components of desmosomes.⁵ Heterozygous *DSG2* knock-outs (KO) are viable and do not develop overt AC under standard animal housing conditions.¹⁸ Subsequently, mice were generated overexpressing murine mutant Dsg2 N271S corresponding to the pathogenic human Dsg2 N266S mutation.¹¹ The mutation is localized in the second extracellular calcium-binding pocket presumably contributing to Dsg2's adhesive function. These mice developed, in contrast to mice overexpressing the same amount of Dsg2 WT, symptoms of AC including biventricular dilation, calcifying necrosis with replacement fibrosis, conduction defects and arrhythmia occasionally resulting in premature death.¹¹ Later on, a knock-in mouse model was described producing mutant Dsg2 with a deletion in the extracellular domains EC1-EC2. Live-born homozygous *DSG2*^{MT} carriers developed an AC-like phenotype during adolescence.^{19,20} The deleted part of Dsg2 includes the most aminoterminal calcium binding site and is believed to be important for adhesion through homo- and heterophilic desmosomal cadherin interaction.²¹ Thus, peptides taken from this domain prevent Dsg2-dependent adhesion²² and autoantibodies targeting the corresponding region in Dsg3 induce cell

dissociation in pemphigus vulgaris.²³

Taken together, neither overexpression nor ~50% reduction of wild type Dsg2 induces overt cardiomyopathy.^{11,18} But overexpression of mutant Dsg2 N271S in the presence of normal wild type Dsg2 levels leads to dose-dependent cardiomyopathy.^{11,24} In contrast, heterozygous mice with only one *DSG2*^{WT} and one *DSG2*^{MT} allele appear to be healthy, although a slight upregulation in transcription of the stress-response genes ANF and BNF were detected at early disease stages.²⁰ Furthermore, complete replacement of two *DSG2*^{WT} by two *DSG2*^{MT} alleles leads to a ~75% reduction in Dsg2 protein expression and a pronounced AC-like phenotype.^{19,20} These observations may be explained either by loss of Dsg2-dependent adhesion and/or by altered cytoplasmic binding of the mutant Dsg2 to signaling molecules. To find out which mechanism is responsible for AC induction, we prepared cardiomyocyte-specific DSG2 knock-out mice and compared the phenotype to that observed in *DSG2*^{MT} mice.

Materials and Methods

DNA cloning and generation of knockout mice

Standard methods were used for targeting construct preparation, transfection, selection and characterization of embryonic stem (ES) cell clones, blastocyst injection and mouse breeding (details in Supplemental Material). The animal experiments were approved by the Landesamt für Natur, Umwelt und Verbraucherschutz (LANUV) Nordrhein-Westfalen under the reference number 8.87-50.10.37.09.114.

RNA isolation, reverse transcription and qRT-PCR

Total RNA was isolated from fresh tissue for preparation of cDNA and PCR amplification as specified in Supplemental Material.

Immunoblotting

Total protein extracts of fresh heart tissue were analyzed by immunoblotting as described in Supplemental Material.

Histological stains and immunohistology

Heart tissue was fixed in 4% formaldehyde/PBS for 12 h and subsequently embedded in paraffin. Sections were prepared and either Azan- or von Kossa-stained.

For immunofluorescence, sections were heated in citrate buffer (pH 6.0) in a pressure cooker for 3 min. Primary antibodies diluted in PBS/1.5% BSA were applied overnight at 4°C: polyclonal rabbit anti-Dsg2 (1:500; Dsg2 IC),²⁰ guinea pig-anti desmoplakin (1:1000; DP-1, Progen), mouse anti-Pkp2 (1:12; 651101, Progen), goat anti-Pg (1:75; sc-30997, Santa Cruz) and rabbit anti-Cx43 (1:1000; C6219, Sigma). Three 5 min washings in modified TBST (50 mM Tris-HCl [pH 7.5], 0.3 M NaCl; 0.05% Tween 20) were followed by secondary antibody incubation for one hour at room temperature (goat anti-rabbit [A-11070], goat anti-mouse [A-11029], donkey anti-goat [A-21432] antibodies conjugated with Alexa488 and goat anti-guinea pig conjugated with Alexa555 [A-21435]; all from Invitrogen; diluted 1:500 in PBS with 1.5% BSA). Sections were washed three times in modified TBST. Background reduction was achieved by 30 min incubation in 0.1% Sudan Black D/70% ethanol. Afterwards slides were washed three times in modified TBST and mounted in Mowiol 4-88 (Roth). Fluorescence micrographs were recorded with an Apotome (Zeiss).

Electron microscopy

Prior to removal, the ventricular myocardium was relaxed by retrograde perfusion with 4-5 ml relaxation buffer (30 mM KCl, 300 mM glucose). Heart samples were cut into cubes of ~1 mm³ in fixative (3.7% formaldehyde, 1% glutaraldehyde, 11.6 g NaH₂PO₄H₂O and 2.7 g NaOH per

liter of ddH₂O) and incubated for 2 h at room temperature. Incubations in 1% OsO₄ for one hour and in 0.5% uranylacetate/0.05 M sodium maleate buffer (pH 5.2) for 2 hours followed. Samples were dehydrated and embedded in araldite (48 h, 60°C) using acetone as intermedium. Ultrathin sections with a thickness of 65 to 75 nm were prepared and contrast was enhanced by treatment with 3% uranylacetate for 4 min followed by 3 min incubation in 80 mM lead citrate solution. Micrographs were recorded on an EM 10 (Zeiss) upgraded with a digital camera (Olympus) using iTEM software (Olympus).

Electrocardiography

Conscious mice were placed on an ECGenie unit (Mouse Specifics Inc.) and signals were recorded for 10 min. The best traces, each containing at least 10 cardiac cycles, were selected and analyzed using the ECGenie software.

Statistical methods

All results are presented as mean \pm SD. The mean of data gathered from one animal was counted as one n. Datasets were tested for Gaussian distribution with the D'Agostino and Pearson omnibus normality test. When datasets were not Gaussian distributed, nonparametric statistical tests were used. Statistical analyses comparing two groups with each other were performed with either two-tailed Mann-Whitney test or two-tailed t-test using 95% confidence intervals.

Statistical analyses comparing three groups were accomplished by either the Kruskal-Wallis test together with the Dunns post hoc test or the ANOVA analysis together with the Bonferroni post hoc test using 95% confidence intervals. All statistical analyses were performed with GraphPad PRISM. * indicates results with $p \leq 0.05$, ** indicates $p \leq 0.01$ and *** indicates $p \leq 0.001$.

Results

Conditional depletion of desmoglein 2 in cardiomyocytes

To prepare mice with a cardiomyocyte-specific *DSG2* knock-out, we made use of a Myh6-driven Cre²⁵ to delete exons 4 and 5 of a floxed *DSG2* allele (Figure 1A). First, using a targeting construct six recombinant AB2.2 ES cell clones were isolated. Correct recombination was detected in two clones by Southern blotting using 5'-external, internal and 3'-external probes (Figure 1A, B). They were injected into C57BL/6J morulae and blastocysts for transgenic line production. Transgenic animals were healthy and the neomycin resistance gene was successfully removed by breeding with Flp⁰-deleter mice.²⁶ For cardiomyocyte-specific *DSG2* inactivation, mice with the floxed *DSG2* alleles were mated with Myh6-Cre transgenic mice,²⁵ which have been shown to initiate cardiac Cre-expression at embryonic day 7 (E7) resulting in efficient recombination of a reporter gene at E9 throughout the myocardium.²⁷ PCR analyses of four animals confirmed correct recombination (Figure 1C). It was, however, difficult to deduce recombination efficiency, since the cardiac tissue samples contain non-cardiomyocytes such as fibroblasts, endothelial cells, smooth muscle cells, and immune cells all of which are not targeted by the Cre recombinase and do not express *Dsg2*. RT-PCR was therefore performed to assess the efficiency of *DSG2*^{WT} mRNA depletion. *DSG2*^{WT} mRNA was reduced to less than 2% in *DSG2*^{CKO} samples (Figure 1D). Instead, a shortened mRNA fragment was amplified. It encodes a non-functional aminoterminal polypeptide of only 80 amino acids consisting of the 29 amino acid signal peptide, the 25 amino acid pro-sequence, 24 amino acids of the extracellular domain EC1 and the two carboxyterminal amino acids histidine and leucine because of erroneous splicing of exon 3 onto exon 6. The processed carboxyterminal 26 amino acid peptide encompassing the W2 adhesion site, which is non-functional in *Dsg2*,²⁸ may still be secreted. Of

note, an additional unexpected mRNA species was amplified by RT-PCR from *DSG2*^{cKO} samples (* in Figure 1D). Upon sequencing, it turned out to be a splice variant, in which 98 bp of *DSG2* intron 3 (5'-ATT GGT TTA GTG GGG AAG CTT CAG GCT CGT GTG GAG GTC AGA GAA CAG CAG TGA GAG TGT CTC TCC CTC TGC CAT GTG TGT TCC AGG ACT GCA CTC AG-3') remain between exons 3 and 6. This leads to an extension of exon 3 coding for the additional 16 amino acids GLVGKLQARVEVREQQ before a stop codon prevents further translation. Taken together both mRNA transcripts result in non-functional, presumably secreted peptides of 26 and 42 amino acids, respectively.

Next, Dsg2 protein expression was examined in *DSG2*^{cKO} heart tissue. As expected, an approximately 50% reduction was noted in heterozygous *DSG2*^{WT/cKO} and less than 3% Dsg2 were detectable in homozygous *DSG2*^{cKO/cKO} (n=4) using two different antibodies directed against cytoplasmic epitopes of Dsg2 (Figure 2A). These results were confirmed by immunohistology (Figure 2C, D). Of note, expression and ID localization of other desmosomal proteins such as Dsp, Pg and Pkp2 were not visibly affected (Figures 2B, E-H; n=4). Nuclear or non-junctional plasma membrane staining was not seen for any of these antigens. Taken together, we conclude that Myh6-Cre-induced *DSG2*^{cKO} results in efficient inhibition of Dsg2 protein expression in the hearts of transgenic mice without significantly affecting the expression level and localization of other major desmosomal proteins.

Gross morphological manifestation of cardiomyopathy

Breeding heterozygous Myh6-Cre carriers with Myh6-Cre-negative mice in a homozygous *DSG2*^{flox/flox} background resulted in 40% *DSG2*^{cKO/cKO} progeny instead of the expected 50% at 4 weeks after birth (n=182). This situation is less dramatic than that encountered in *DSG2*^{MT} mice expressing Dsg2 mutants lacking parts of their adhesive EC1-EC2 domains. In that instance only

15% of the expected homozygous mutants were found at 4 weeks (n=104). Remarkably, most newborn mice appeared to be healthy in both situations. Myocardial alterations, however, became visible in all homozygous $DSG2^{cKO}$ and $DSG2^{MT}$ animals by the age of 4-6 weeks, i.e. towards the end of postnatal heart growth (Figure S1D). Most conspicuous were white, non-transparent and differently sized areas on the cardiac surface occurring in the majority of $DSG2^{MT}$ and $DSG2^{cKO}$ mice (Figure 3K, L; Figure S1B, C). Such lesions, which were never seen in $DSG2^{WT}$ animals, localized in 60% on the anterolateral surface of the left ventricle near the apex of $DSG2^{MT}$ hearts (n=79; see also²⁰). In addition, regions were noted, in which the convex and light red-colored even surface, which is typically encountered in the $DSG2^{WT}$ heart, was substituted by an uneven patchy dark red-colored surface (arrowheads in Figure 3I, J). Such alterations are characteristic features of wall thinning and aneurysms. Accordingly, enlargement of the right ventricle and both atria were observed (Figure S1). Taken together, visual inspection of the dissected hearts sufficed to detect pathological anomalies in almost 100% of $DSG2^{MT}$ and $DSG2^{cKO}$ animals by 4 weeks (Figure S1D).

Histological detection of calcifying replacement fibrosis and interstitial fibrosis

To further compare cardiac pathology between $DSG2^{MT}$ and $DSG2^{cKO}$ animals, detailed histological analyses were performed. Transmural fibrotic foci corresponding to the macroscopically visible surface lesions were detected by Azan staining (arrows in Figure 3C, C', F, F'). Many of them contained calcifications as determined by von Kossa-staining in both genetic situations (arrows in corresponding sections shown in Figure 4C, C', F, F'). Careful examination revealed von Kossa-positive foci in up to a 100% of animals by 6 weeks. Ultrastructurally, remnants of cardiomyocytes were detected that were surrounded by calcified material (Figure 4G, H) providing evidence for cardiomyocyte necrosis, which has been

identified as a key event in the pathogenesis of murine AC.¹¹ Calcification, however, was not detectable in all lesions (arrowheads in Figure 3B, B', E, E' and arrowheads in corresponding areas of adjacent sections shown in Figure 4B, B', E, E'). These von Kossa-negative lesions likely contribute to the continuously increasing interstitial fibrosis observed in murine AC hearts.¹⁹ Taken together, the different types of fibrotic lesions are identical in *DSG2*^{ckO} and *DSG2*^{MT} hearts. Furthermore, comparable lesions have been identified in human AC patients with *DSG2* mutations.^{8,10}

Disease stages

Gross morphological appearance and histology of most hearts was normal at 2 weeks (Figures S1, S2, S3). Only two weeks later visible changes such as cardiomegaly and/or surface lesions with a preference for the right ventricle had developed (Figure S1). At this time, the mRNA of the stress-response genes ANF (1.03 ± 0.28 in *DSG2*^{WT} versus 12.80 ± 8.75 in *DSG2*^{ckO}), GDF15 (1.45 ± 1.17 in *DSG2*^{WT} versus 9.04 ± 6.55 in *DSG2*^{ckO}) and CTGF (1.03 ± 0.29 *DSG2*^{WT} versus 2.58 ± 1.20 in *DSG2*^{ckO}) was significantly elevated in *DSG2*^{ckO} (for all genes: n=4, p=0.0286; for *DSG2*^{MT} see²⁰). The initial lesions contained necrotic cardiomyocytes and little collagen deposits (Figure S2). At the same time, cell-rich infiltrates containing CD45-positive immune cells appeared in the lesions (Figure 5C, E). Furthermore, von Kossa-positive calcinosis was detectable in some lesions (Figure S3). Increased collagen fiber deposition was noted by 6-12 weeks (Figures S2), which was accompanied by a reduction in CD45 cells (Figure 5D, F) in lesioned areas. In contrast, von Kossa-positive foci persisted (Figure S3). These observations show that the timing and stages of disease progression of the newly established *DSG2*^{ckO} mice is indistinguishable from that observed in *DSG2*^{MT} animals.

Loss of desmosome-like structures and intercalated disc dissociation

To further work out the resemblance between *DSG2*^{cKO} and *DSG2*^{MT} hearts at the ultrastructural level, electron microscopy was performed. For best evaluation, the myocardium was relaxed prior to fixation. Morphology and organization of sarcomeres were not visibly altered in longitudinal sections of intact cardiomyocytes. Cell-cell contact regions contained normal-appearing fasciae adhaerentes and adjacent gap junctions. Desmosome-like structures were frequently observed in IDs of wild type control mice (arrows in Figure 6A, A'), but were not seen in IDs of *DSG2*^{cKO} and *DSG2*^{MT} mice (Figure 6B-C').

Although intercellular gap width was not altered in most instances, dissociation of IDs was occasionally noted in the mutant hearts (Figure 6D, E) resulting in remnant junctions with adhering actin filaments. Adjacent cytoplasmic regions appeared to be disordered with multiple membranous structures and disarranged mitochondria. The disconnected intercellular gaps were usually filled with membranes and included large cytoplasmic organelles such as mitochondria in some instances. In regions directly adjacent to fibrotic lesions sarcomeres ended in membrane regions that were decorated by scarce plaque material and bordered directly to the collagen fiber-rich extracellular matrix (Figure 6F, G).

Altered conduction and connexin 43 distribution

To examine electrophysiological alterations, electrocardiography was performed using the ECGenie system (Figure 7E, F). Despite normal heart rates (RR-intervals), highly significant prolonged PR and QRS intervals were detected in both the *DSG2*^{MT} (n=6) vs. *DSG2*^{WT} (n=8) and *DSG2*^{cKO} (n=8) vs. *DSG2*^{flox(E4-5)} control mice (n=10) indicating conduction defects of atria and ventricles. We therefore investigated the expression of the major myocardial gap junction protein connexin 43. Overall protein levels were similar in matched mutant and wild type hearts

(Figure 7 D). Immunolocalization (n=5), however, revealed that connexin 43-staining was not restricted to IDs in *DSG2*^{ckO} and *DSG2*^{MT} but was also detectable in multiple puncta in the cytoplasm of perilesional cardiomyocytes (Figure 7 A-C).

Discussion

We report on the establishment and characterization of a mouse model, in which, for the first time, a desmosomal cadherin was tissue-specifically ablated in a specialized cell type, namely the cardiomyocyte. The birth of viable animals with inconspicuous gross heart morphology provides evidence that *Dsg2* is not essential for growth and function of the heart during late embryogenesis and early postnatal life. This is remarkable, since *Dsg2* is by far the major *Dsg* isoform expressed in cardiomyocytes.⁵

All analyses performed in this study reveal a striking phenotypic resemblance between *DSG2*^{ckO} and *DSG2*^{MT} mice. This includes aspects of disease onset and progression, histological features, ultrastructural disturbances and functional deficiencies. Furthermore, our observations are similar to those reported for mice overexpressing *Dsg2* N271S.¹¹ We therefore suggest that the same pathways induce cardiomyopathy in all three models.

The observed widening and/or dissociation of intercalated discs in all three *DSG2*-mutant mouse strains (^{19,24} and this study) presents strong *in vivo* evidence for compromised adhesion. Similar changes were noted in hearts of patients with *Dsg2*-related AC.^{10,12,29} *In vitro* experimentation further supports an adhesive function of *Dsg2*. Expression of different human AC-related *Dsg2* mutants and inhibition of *Dsg2* adhesion were reported to reduce adhesion upon expression in HL-1 cardiomyocytes²² (for contrasting results on another mutant see ³⁰). The situation in other AC types is less clear. While some reports support an adhesion deficiency as evidenced by intercalated disc widening and dissociation in murine AC models,³¹ in patient-

derived iPSCs³² and in patients,²⁹ a recent publication portrays a more complex situation.³³ Depletion of either plakoglobin or plakophilin resulted in weakened cell-cell adhesion as was observed by others before^{34,35} whereas mutant polypeptides did not (for contrasting results, see, however, ³⁴). Instead, they reported on an abnormal shear stress response.³³ Given the apparent differences in the various AC disease forms and model systems we may have to consider the disconcerting possibility that in the different scenarios the initial molecular pathomechanisms differ and merge only later in common pathways to induce the full AC phenotype.

We find it quite remarkable that desmosomal proteins are still efficiently recruited to and remain associated with the ID in the absence of Dsg2. In contrast, Pg depletion results in considerable loss of Dsg2, Pkp2 and Dsp at the ID.^{36,37} Similarly, Pkp2 is needed for junctional localization of Dsp and Dsg2 in embryonic heart.³⁸ The lack of desmosome-like structures in *DSG2*^{cKO} hearts, however, shows that Dsc2 is not able to fully compensate for the loss of Dsg2. Clearly, both cadherins are not interchangeable as is evident from the lack of overt cardiomyopathy in desmocollin 2 knockout mice.³⁹ The clinical manifestation of an AC-like phenotype during the postnatal growth period of young *DSG2*^{cKO} mice assigns an important function to Dsg2 in supporting the increasing work load of the growing heart. Yet, 50% reduction of Dsg2 in *DSG2*^{WT/KO} and *DSG2*^{WT/cKO} mice still supports overall normal heart function (this study and ¹⁸), although physical challenges may induce AC symptoms as has been observed in heterozygous Pg KO mice.⁴⁰ In the situation of homozygous *DSG2*^{MT} mice both the adhesion defect of the mutant polypeptide and the reduction of the mutant Dsg2 to ~25% likely contribute to AC-like pathogenesis.²⁰ The new *DSG2*^{cKO} mouse model provides proof that down regulation of Dsg2 below a critical level induces a cardiomyopathy that is very similar to that observed in *DSG2*^{MT} mice.

Of note, not only Dsg2 reduction but also overexpression of Dsg2 N271S leads to cardiomyopathy. Since overexpression of wild type Dsg2 alone does not induce cardiomyopathy, one has to conclude that Dsg2 N271S interferes with wild type Dsg2 function by a dominant negative mechanism¹¹. Interestingly, high overexpression results in a more severe phenotype than low overexpression.¹¹ Given that Dsg2 N271S induces an AC-like phenotype in the presence of wild type Dsg2, it is not clear, why Dsg2 lacking the EC1-EC2 domains does not. Reasons for this discrepancy may be that deletion of the EC1-EC2 segment is less severe than the single amino acid change in the Dsg2 N271S, or that the level of mutant protein expression is relevant for disease development. In all instances, interference appears to occur at the ID, since mutant Dsg2 is efficiently localized to the ID in the different murine models and human Dsg2-related AC.^{8,11,20,30,41}

Multiple studies have assigned a crucial role of plakoglobin signaling to the initiation of AC in mouse and man.^{17,42-44} Comparing disease manifestation with the available binding sites of desmosomal cadherins for Pg or other desmosomal cadherin-dependent signaling molecules in the various murine models, however, shows that there is no clear correlation (Figure 8). We therefore conclude that altered Dsg2 cytoplasmic tail-dependent signaling, which relies on Pg displacement from the desmosome, is unlikely the major disease mechanism. This is also supported by AC development either in the absence of Pg^{36,37} or with unperturbed Pg expression in the ID.⁴⁵ Instead, compromised desmosomal cadherin-mediated adhesion may be at the core of disease initiation. This concept is strongly supported by the loss-of-function phenotype observed in the present study. It is indirectly supported by the observation that AC-associated Dsg2 mutations in the intracellular catenin-binding domain do not compromise Pg- or Pkp2- binding.⁸

It is of interest to note that Dsg2 reduction has also been observed in the hearts of

PKP2^{KO/KO} embryos,³⁸ in heart-specific homozygous Pg knock-outs (*JUP*^{cKO/cKO})^{36,37} and in the presence of normal Pg ID expression in a heart-specific Dsp knock-out.⁴⁵ Similar to the observations reported here, a selective loss of desmosome-like structures but not of adherens junctions and gap junctions was detected in the *JUP*^{cKO/cKO}.^{36,37} In addition, Dsg2 downregulation has also been observed in human AC patients independent of the underlying mutations, even in the presence of normal Pg localization to IDs.⁴⁶ A provocative conclusion is that down regulation of Pg and Pkp2 may also lead to weakening of desmosomal cadherin-mediated adhesion and desmin intermediate filament anchorage. *DSP* mutations^{31,45} and certain desmin mutations^{47,48} may contribute in a similar fashion to impair the stability and resilience of the desmosome-based transcellular scaffold. Thus, altered adhesion may be the primary dysfunction of desmosome-related cardiomyopathy that can be brought about in different ways as reflected by the different desmosomal gene mutations reported to date.

Limitations

Murine models of human AC present significant limitations given the differences in genetics, life span, immune response, epicardial fat and secondary reactions such as fibrotic scar formation with calcinosis typical in mice⁴⁹ versus fibrotic replacement in human with variable amounts of adipose tissue.⁵⁰ In addition, several aspects of our murine AC models remain to be explored. These include the analysis of embryonic lethality, detailed statistics of survival, examination of the effect of physical activity on modulating disease progression in homozygous mutants and, even more, the induction of disease symptoms in heterozygotes.

Acknowledgments: We thank Vanessa Creutz, Ursula Wilhelm, Sabine Eisner, Marina Lürkens Weber and Tanja Tropartz for expert technical support, Katharina Stracke for RT-PCR analyses, Dr. Schneider (Imperial College London) for Myh6-Cre mice and Dr. Anastassiadis (Dresden University) for Flp^o-mice. This work was supported by the transgenic service, a core facility of

the Interdisciplinary Center for Clinical Research (IZKF) Aachen within the Faculty of Medicine at RWTH Aachen University.

Funding Source: This work was supported by a grant from the German Research Council (LE 566/11-1) and the IZKF.

Conflict of Interest Disclosures: None.

References:

1. Romero J, Mejia-Lopez E, Manrique C, Lucariello R. Arrhythmogenic right ventricular cardiomyopathy (arvc/d): A systematic literature review. *Clin Med Insights Cardiol.* 2013;7:97-114.
2. Awad MM, Calkins H, Judge DP. Mechanisms of disease: Molecular genetics of arrhythmogenic right ventricular dysplasia/cardiomyopathy. *Nat Clin Pract Cardiovasc Med.* 2008;5:258-267.
3. Franke WW, Borrmann CM, Grund C, Pieperhoff S. The area composita of adhering junctions connecting heart muscle cells of vertebrates. I. Molecular definition in intercalated disks of cardiomyocytes by immunoelectron microscopy of desmosomal proteins. *Eur J Cell Biol.* 2006;85:69-82.
4. Harmon RM, Green KJ. Structural and functional diversity of desmosomes. *Cell Commun Adhes.* 2013;20:171-187.
5. Holthofer B, Windoffer R, Troyanovsky S, Leube RE. Structure and function of desmosomes. *Int Rev Cytol.* 2007;264:65-163.
6. Awad MM, Dalal D, Cho E, Amat-Alarcon N, James C, Tichnell C, et al. Dsg2 mutations contribute to arrhythmogenic right ventricular dysplasia/cardiomyopathy. *Am J Hum Genet.* 2006;79:136-142.
7. Fressart V, Duthoit G, Donal E, Probst V, Deharo JC, Chevalier P, et al. Desmosomal gene analysis in arrhythmogenic right ventricular dysplasia/cardiomyopathy: Spectrum of mutations and clinical impact in practice. *Europace.* 2010;12:861-868.
8. Gehmlich K, Asimaki A, Cahill TJ, Ehler E, Syrris P, Zachara E, et al. Novel missense mutations in exon 15 of desmoglein-2: Role of the intracellular cadherin segment in arrhythmogenic right ventricular cardiomyopathy? *Heart Rhythm.* 2010;7:1446-1453.

9. Gehmlich K, Lambiase PD, Asimaki A, Ciaccio EJ, Ehler E, Syrris P, et al. A novel desmocollin-2 mutation reveals insights into the molecular link between desmosomes and gap junctions. *Heart Rhythm*. 2011;8:711-718.
10. Pilichou K, Nava A, Basso C, Beffagna G, Bauce B, Lorenzon A, et al. Mutations in desmoglein-2 gene are associated with arrhythmogenic right ventricular cardiomyopathy. *Circulation*. 2006;113:1171-1179.
11. Pilichou K, Remme CA, Basso C, Campian ME, Rizzo S, Barnett P, et al. Myocyte necrosis underlies progressive myocardial dystrophy in mouse *dsg2*-related arrhythmogenic right ventricular cardiomyopathy. *J Exp Med*. 2009;206:1787-1802.
12. Posch MG, Posch MJ, Perrot A, Dietz R, Ozcelik C. Variations in *dsg2*: V56m, v158g and v920g are not pathogenic for arrhythmogenic right ventricular dysplasia/cardiomyopathy. *Nat Clin Pract Cardiovasc Med*. 2008;5:E1.
13. Rigato I, Bauce B, Rampazzo A, Zorzi A, Pilichou K, Mazzotti E, et al. Compound and digenic heterozygosity predicts lifetime arrhythmic outcome and sudden cardiac death in desmosomal gene-related arrhythmogenic right ventricular cardiomyopathy. *Circ Cardiovasc Genet*. 2013;6:533-542.
14. Syrris P, Ward D, Asimaki A, Evans A, Sen-Chowdhry S, Hughes SE, et al. Desmoglein-2 mutations in arrhythmogenic right ventricular cardiomyopathy: A genotype-phenotype characterization of familial disease. *Eur Heart J*. 2007;28:581-588.
15. Xu T, Yang Z, Vatta M, Rampazzo A, Beffagna G, Pilichou K, et al. Compound and digenic heterozygosity contributes to arrhythmogenic right ventricular cardiomyopathy. *J Am Coll Cardiol*. 2010;55:587-597.
16. Chen SN, Gurha P, Lombardi R, Ruggiero A, Willerson JT, Marian AJ. The hippo pathway is activated and is a causal mechanism for adipogenesis in arrhythmogenic cardiomyopathy. *Circ Res*. 2014;114:454-468.
17. Garcia-Gras E, Lombardi R, Giocondo MJ, Willerson JT, Schneider MD, Khoury DS, et al. Suppression of canonical wnt/beta-catenin signaling by nuclear plakoglobin recapitulates phenotype of arrhythmogenic right ventricular cardiomyopathy. *J Clin Invest*. 2006;116:2012-2021.
18. Eshkind L, Tian Q, Schmidt A, Franke WW, Windoffer R, Leube RE. Loss of desmoglein 2 suggests essential functions for early embryonic development and proliferation of embryonal stem cells. *Eur J Cell Biol*. 2002;81:592-598.
19. Kant S, Krull P, Eisner S, Leube RE, Krusche CA. Histological and ultrastructural abnormalities in murine desmoglein 2-mutant hearts. *Cell Tissue Res*. 2012;348:249-259.

20. Krusche CA, Holthofer B, Hofe V, van de Sandt AM, Eshkind L, Bockamp E, et al. Desmoglein 2 mutant mice develop cardiac fibrosis and dilation. *Basic Res Cardiol*. 2011;106:617-633.
21. Al-Amoudi A, Diez DC, Betts MJ, Frangakis AS. The molecular architecture of cadherins in native epidermal desmosomes. *Nature*. 2007;450:832-837.
22. Schlipp A, Schinner C, Spindler V, Vielmuth F, Gehmlich K, Syrris P, et al. Desmoglein-2 interaction is crucial for cardiomyocyte cohesion and function. *Cardiovasc Res*. 2014;104:245-257.
23. Tsunoda K, Ota T, Aoki M, Yamada T, Nagai T, Nakagawa T, et al. Induction of pemphigus phenotype by a mouse monoclonal antibody against the amino-terminal adhesive interface of desmoglein 3. *J Immunol*. 2003;170:2170-2178.
24. Rizzo S, Lodder EM, Verkerk AO, Wolswinkel R, Beekman L, Pilichou K, et al. Intercalated disc abnormalities, reduced na(+) current density, and conduction slowing in desmoglein-2 mutant mice prior to cardiomyopathic changes. *Cardiovasc Res*. 2012;95:409-418.
25. Agah R, Frenkel PA, French BA, Michael LH, Overbeek PA, Schneider MD. Gene recombination in postmitotic cells. Targeted expression of cre recombinase provokes cardiac-restricted, site-specific rearrangement in adult ventricular muscle in vivo. *J Clin Invest*. 1997;100:169-179.
26. Kranz A, Fu J, Duerschke K, Weidlich S, Naumann R, Stewart AF, et al. An improved flp deleter mouse in c57bl/6 based on flpo recombinase. *Genesis*. 2010;48:512-520.
27. de Lange FJ, Moorman AF, Anderson RH, Manner J, Soufan AT, de Gier-de Vries C, et al. Lineage and morphogenetic analysis of the cardiac valves. *Circ Res*. 2004;95:645-654.
28. Lowndes M, Rakshit S, Shafraz O, Borghi N, Harmon RM, Green KJ, et al. Different roles of cadherins in the assembly and structural integrity of the desmosome complex. *J Cell Sci*. 2014;127:2339-2350.
29. Basso C, Czarnowska E, Della Barbera M, Bauce B, Beffagna G, Wlodarska EK, et al. Ultrastructural evidence of intercalated disc remodelling in arrhythmogenic right ventricular cardiomyopathy: An electron microscopy investigation on endomyocardial biopsies. *Eur Heart J*. 2006;27:1847-1854.
30. Gaertner A, Klauke B, Stork I, Niehaus K, Niemann G, Gummert J, et al. In vitro functional analyses of arrhythmogenic right ventricular cardiomyopathy-associated desmoglein-2-missense variations. *PLoS One*. 2012;7:e47097.
31. Yang Z, Bowles NE, Scherer SE, Taylor MD, Kearney DL, Ge S, et al. Desmosomal dysfunction due to mutations in desmoplakin causes arrhythmogenic right ventricular dysplasia/cardiomyopathy. *Circ Res*. 2006;99:646-655.

32. Caspi O, Huber I, Gepstein A, Arbel G, Maizels L, Boulos M, et al. Modeling of arrhythmogenic right ventricular cardiomyopathy with human induced pluripotent stem cells. *Circ Cardiovasc Genet*. 2013;6:557-568.
33. Hariharan V, Asimaki A, Michaelson JE, Plovie E, MacRae CA, Saffitz JE, et al. Arrhythmogenic right ventricular cardiomyopathy mutations alter shear response without changes in cell-cell adhesion. *Cardiovasc Res*. 2014;104:280-289.
34. Sato PY, Coombs W, Lin X, Nekrasova O, Green KJ, Isom LL, et al. Interactions between ankyrin-g, plakophilin-2, and connexin43 at the cardiac intercalated disc. *Circ Res*. 2011;109:193-201.
35. Huang H, Asimaki A, Lo D, McKenna W, Saffitz J. Disparate effects of different mutations in plakoglobin on cell mechanical behavior. *Cell Motil Cytoskeleton*. 2008;65:964-978.
36. Li D, Liu Y, Maruyama M, Zhu W, Chen H, Zhang W, et al. Restrictive loss of plakoglobin in cardiomyocytes leads to arrhythmogenic cardiomyopathy. *Hum Mol Genet*. 2011;20:4582-4596.
37. Li J, Swope D, Raess N, Cheng L, Muller EJ, Radice GL. Cardiac tissue-restricted deletion of plakoglobin results in progressive cardiomyopathy and activation of β -catenin signaling. *Mol Cell Biol*. 2011;31:1134-1144.
38. Grossmann KS, Grund C, Huelsken J, Behrend M, Erdmann B, Franke WW, et al. Requirement of plakophilin 2 for heart morphogenesis and cardiac junction formation. *J Cell Biol*. 2004;167:149-160.
39. Rimpler U. Funktionelle charakterisierung von desmocollin 2 während der embryonalentwicklung und im adulten herzen in der maus. Humboldt-Universität zu Berlin. 2014.
40. Kirchhof P, Fabritz L, Zwiener M, Witt H, Schafers M, Zellerhoff S, et al. Age- and training-dependent development of arrhythmogenic right ventricular cardiomyopathy in heterozygous plakoglobin-deficient mice. *Circulation*. 2006;114:1799-1806.
41. Rasmussen TB, Palmfeldt J, Nissen PH, Magnoni R, Dalager S, Jensen UB, et al. Mutated desmoglein-2 proteins are incorporated into desmosomes and exhibit dominant-negative effects in arrhythmogenic right ventricular cardiomyopathy. *Hum Mutat*. 2013;34:697-705.
42. Asimaki A, Tandri H, Huang H, Halushka MK, Gautam S, Basso C, et al. A new diagnostic test for arrhythmogenic right ventricular cardiomyopathy. *N Engl J Med*. 2009;360:1075-1084.
43. Lombardi R, da Graca Cabreira-Hansen M, Bell A, Fromm RR, Willerson JT, Marian AJ. Nuclear plakoglobin is essential for differentiation of cardiac progenitor cells to adipocytes in arrhythmogenic right ventricular cardiomyopathy. *Circ Res*. 2011;109:1342-1353.

44. Lombardi R, Dong J, Rodriguez G, Bell A, Leung TK, Schwartz RJ, et al. Genetic fate mapping identifies second heart field progenitor cells as a source of adipocytes in arrhythmogenic right ventricular cardiomyopathy. *Circ Res*. 2009;104:1076-1084.
45. Lyon RC, Mezzano V, Wright AT, Pfeiffer E, Chuang J, Banares K, et al. Connexin defects underlie arrhythmogenic right ventricular cardiomyopathy in a novel mouse model. *Hum Mol Genet*. 2014;23:1134-1150.
46. Vite A, Gandjbakhch E, Prost C, Fressart V, Fouret P, Neyroud N, et al. Desmosomal cadherins are decreased in explanted arrhythmogenic right ventricular dysplasia/cardiomyopathy patient hearts. *PLoS One*. 2013;8:e75082.
47. Klauke B, Kossmann S, Gaertner A, Brand K, Stork I, Brodehl A, et al. De novo desmin-mutation n116s is associated with arrhythmogenic right ventricular cardiomyopathy. *Hum Mol Genet*. 2010;19:4595-4607.
48. van Tintelen JP, Van Gelder IC, Asimaki A, Suurmeijer AJ, Wiesfeld AC, Jongbloed JD, et al. Severe cardiac phenotype with right ventricular predominance in a large cohort of patients with a single missense mutation in the des gene. *Heart Rhythm*. 2009;6:1574-1583.
49. Brunnert SR, Altman NH. Dystrophic cardiac calcinosis in mice: Abnormal myocardial response to freeze-thaw injury. *Lab Anim Sci*. 1990;40:616-619.
50. Su L, Siegel JE, Fishbein MC. Adipose tissue in myocardial infarction. *Cardiovasc Pathol*. 2004;13:98-102.

Cardiovascular Genetics

Figure Legends:

Figure 1: Cardiomyocyte-specific inactivation of *DSG2* by Myh6-Cre-mediated excision of floxed *DSG2* exons 4-5 in transgenic mice. The scheme in (A) depicts part of the *DSG2*^{WT} allele with exons 2-8 (E2 to E8) that was mutated by homologous recombination introducing loxP sites in exons 4 and 5 and an FRT-site bounded neomycin resistance cassette downstream of exon 5. The resulting allele *DSG2*^{lox(E4-5-neo)} was subsequently modified by Flp⁰-driven excision of the

neomycin resistance cassette (*neo*) producing allele $DSG2^{\text{floxE4-5}}$. Myh6-Cre-mediated recombination led to knockout allele $DSG2^{\text{cKO}}$. Positions of *EcoRV* restriction sites (RV) and probes used for genotyping are demarcated. **(B)** Autoradiographs of Southern blots after hybridization of gel electrophoretically-separated and *EcoRV*-digested DNA from wild type (WT) and recombinant embryonic stem cells (cl 449) with either the 5', internal or 3' probes. Note that in addition to the 15.7 kb *EcoRV* fragment of the wild type allele other signals (5' probe: 7.4 kb; internal probe: 2.3 kb; 3' probe: 5.2 kb) are detected in the recombinant cell clone as predicted for allele $DSG2^{\text{floxE4-5-neo}}$. **(C)** shows Midori Green-stained, electrophoretically-separated DNA fragments that were obtained by PCR amplification of genomic regions surrounding the 5' loxP site. Note that a single 167 bp fragment is amplified from $DSG2^{\text{WT}}$ mice and that an additional fragment is detectable in the heart but not liver of mice that also contain the Myh6-Cre transgene. The size (236 bp) of this fragment corresponds to that expected for the recombined $DSG2^{\text{cKO}}$ allele. Left panel of **(D)** depicts PCR products amplified from cDNA derived from heart tissue of a $DSG2^{\text{floxE4-5}/\text{floxE4-5}}$ mouse (WT/WT), a mouse carrying an additional Myh6-Cre gene (cKO/cKO) and a $DSG2^{\text{floxE4-5}/\text{WT}}$ mouse carrying a Myh6-Cre transgene (WT/cKO). Note that the $DSG2^{\text{WT}}$ mRNA fragment is undetectable in the homozygous $DSG2^{\text{cKO}}$ mouse indicating efficient *DSG2* recombination and altered mRNA production. In addition to the expected fragment reduction by 305 bp, an intermediate fragment was amplified (asterisk) because of incomplete splicing. Right panel in **(D)** presents a histogram of qRT-PCR results detecting $DSG2^{\text{WT}}$ mRNA by amplification of a region encoded by E4-E5 from cardiac RNA (n=4 in each instance). Note that the expression is reduced to $46 \pm 16\%$ in heterozygous $DSG2^{\text{cKO}/\text{WT}}$ (WT/cKO) and that it is almost undetectable ($1.5 \pm 0.6\%$) in homozygous $DSG2^{\text{cKO}}$ (cKO/cKO) mice at 2, 4 or 12 weeks.

Figure 2: Dsg2 depletion and desmosomal protein expression in cardiomyocyte-specific *DSG2^{ckO}* mice. **(A)** Immunoblot detection of Dsg2 using rabbit (upper panel) and guinea pig antibodies (lower panel) in SDS-PAGE separated heart lysates of 12 week-old mice. Anti- β actin antibodies (Actb) were used as controls after stripping. Genotypes were *DSG2^{WT/WT}* (WT/WT); *DSG2^{WT/flox(E4-5)} + Myh6-Cre* (WT/cKO); and *DSG2^{flox(E4-5)/flox(E4-5)} + Myh6-Cre* (cKO/cKO). Note that Dsg2 levels are significantly reduced in heterozygotes (~40%) and almost undetectable in homozygous conditional knockouts. **(B)** shows unchanged levels of plakoglobin (Pg) and desmoplakin (Dsp) in immunoblots (β -actin [Actb] as control). **(C-D'')** Double fluorescence microscopy and corresponding interference contrast images of *DSG2^{WT}* **(C)** and homozygous *DSG2^{ckO}* **(D)** (same genotypes as in **A, B**). Primary antibodies were rabbit anti-Dsg2 **(C, D)** and guinea pig anti-desmoplakin (Dsp; **C', D'**). Note absence of Dsg2 immunoreactivity in the homozygous mutants (arrowheads in **D**) and ID co-localization of Dsg2 and Dsp in the wild type (arrowheads in **C, C'**). **(E-H')** Despite loss of Dsg2 expression, *DSG2^{ckO}* mice show normal ID localization (arrowheads) of Pg **(F)** and Pkp2 **(H)**. The intensity of fluorescence signals is comparable to those of wild type controls **(E, G)** and localization is identical to Dsp **(E', F', G', H')**. Bars: 20 μ m.

Figure 3: Microscopic and macroscopic images of hearts from 12 week-old *DSG2^{WT}*, *DSG2^{MT}* and cardiomyocyte-specific *DSG2^{ckO}* mice. **(A-F')** Histological comparisons of hearts using azan staining. Note the similar phenotypes in *DSG2^{MT}* and *DSG2^{ckO}* presenting pronounced interstitial fibrosis (arrowheads in **B, B', E, E'**) and extensive transmural fibrotic lesions **(C, C', F, F')** that are characterized by necrotic cardiomyocytes (arrows) surrounded by collagen-rich matrix. Bars: 1 mm in **A-C** and **D-F**; 100 μ m in **B', C', E', F'**. **(G-L)** Pronounced right ventricular dilation and

wall thinning (arrowheads) are readily seen in dissected mutant and knockout hearts (**I, J**). In addition, extensive fibrotic foci (arrows) are detected in both mutant strains (**K, L**). Bar: 2 mm in **G**: (same magnification in **J-L**).

Figure 4: Detection of calcinosis in $DSG2^{MT}$ and $DSG2^{cKO}$ hearts. The pictures in **A-F** are serial sections of the corresponding sections shown in Figure 3A-F. (**A-F**) depict von Kossa-stained sections at low magnification at left (bar: 1 mm) and high magnification at right (bars: 100 μ m). Note the absence of calcification in interstitial fibrosis (arrowheads in **B, B', E, E'**) and its presence in extensive transmural fibrotic foci (arrows in **C, C', F, F'**) next to healthy myocardium (My) in $DSG2^{MT}$ and $DSG2^{cKO}$. (**G, H**) The electron micrographs highlight further details of calcifying necrosis with dead cardiomyocytes surrounded by layers of calcified material (stars) and densely-packed collagen fibers (Co). Bar: 1 μ m in **G** (same magnification in **H**).

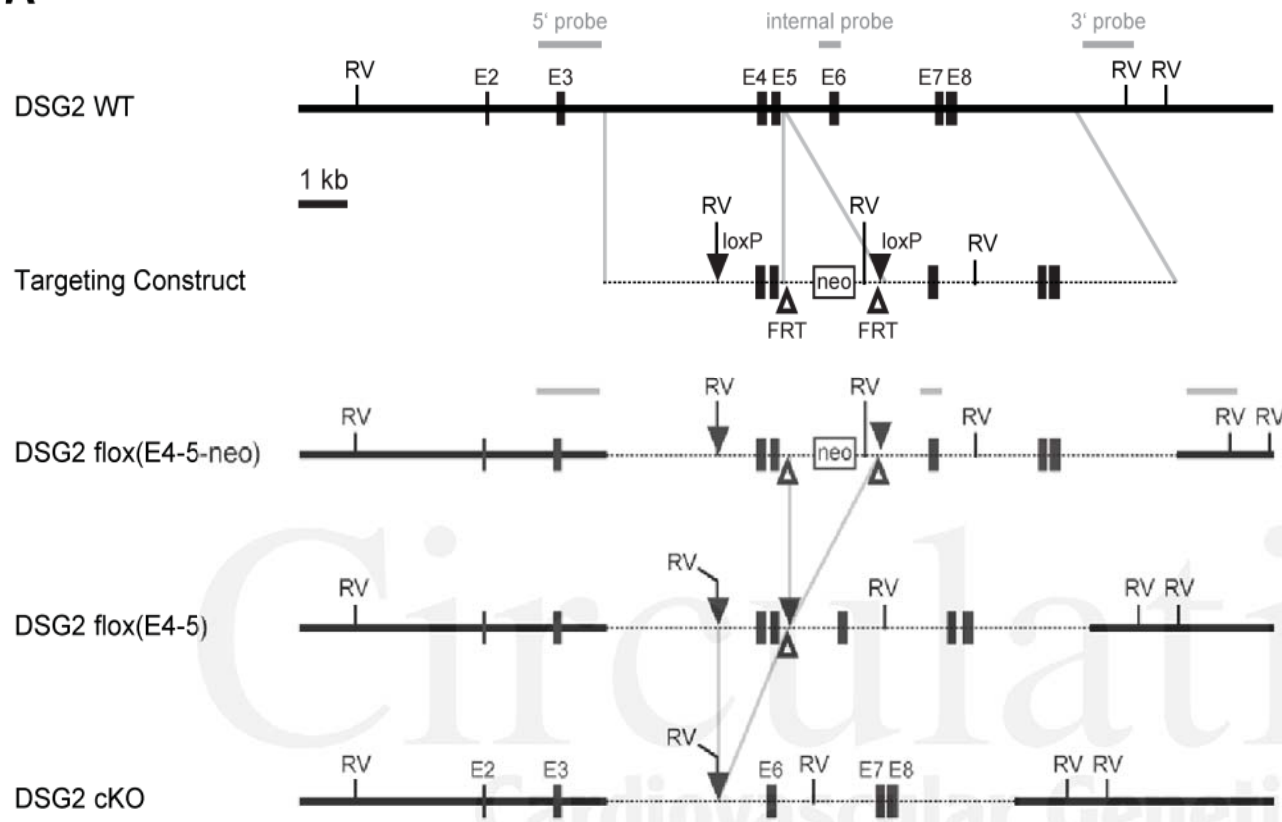
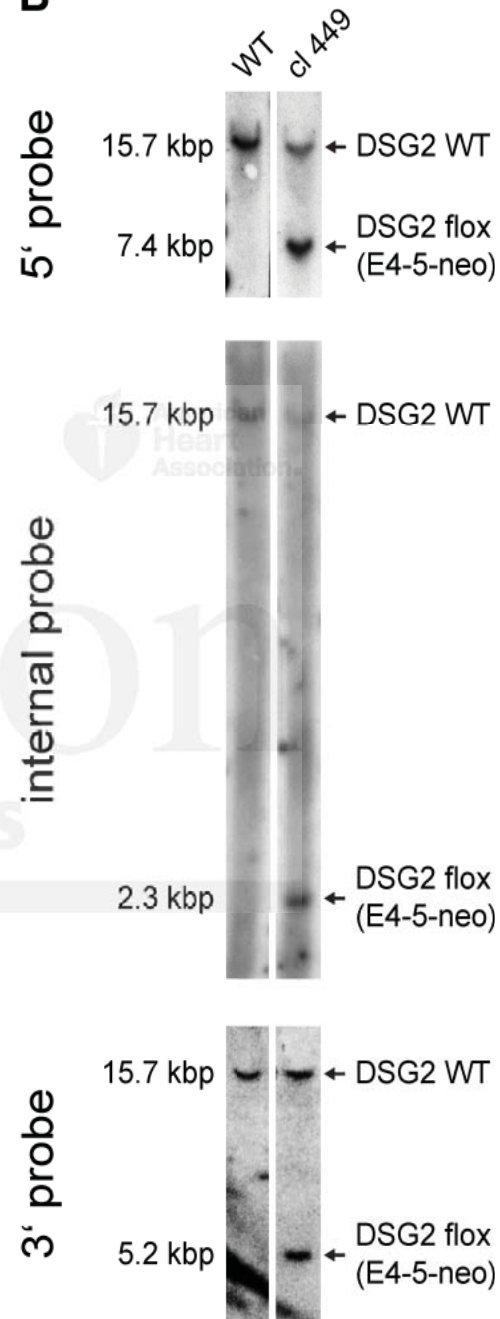
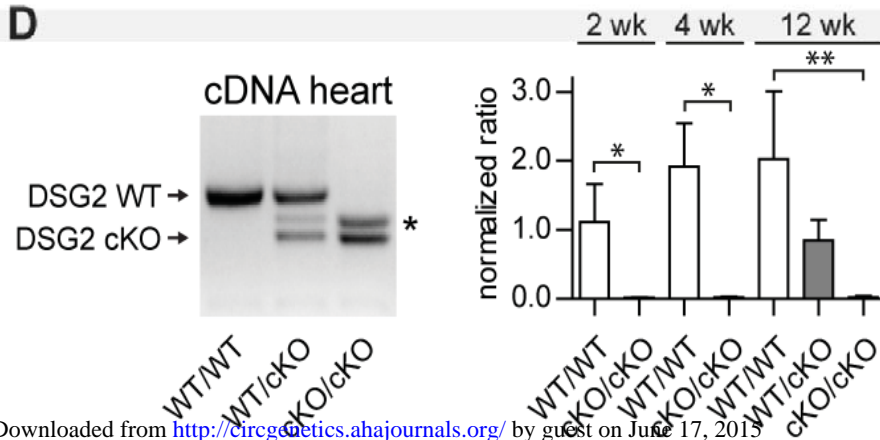
Figure 5: Immunohistological detection of the CD45 antigen in hearts of $DSG2^{WT}$, $DSG2^{MT}$ and $DSG2^{cKO}$ mice. Note the high-degree of CD45-positive immune cells in fibrotic lesions (*) at 4 weeks which decreases considerably by 12 weeks. Arrows denote isolated CD45-positive single cells in normal-appearing myocardium. Bar: 100 μ m (same magnification in all images).

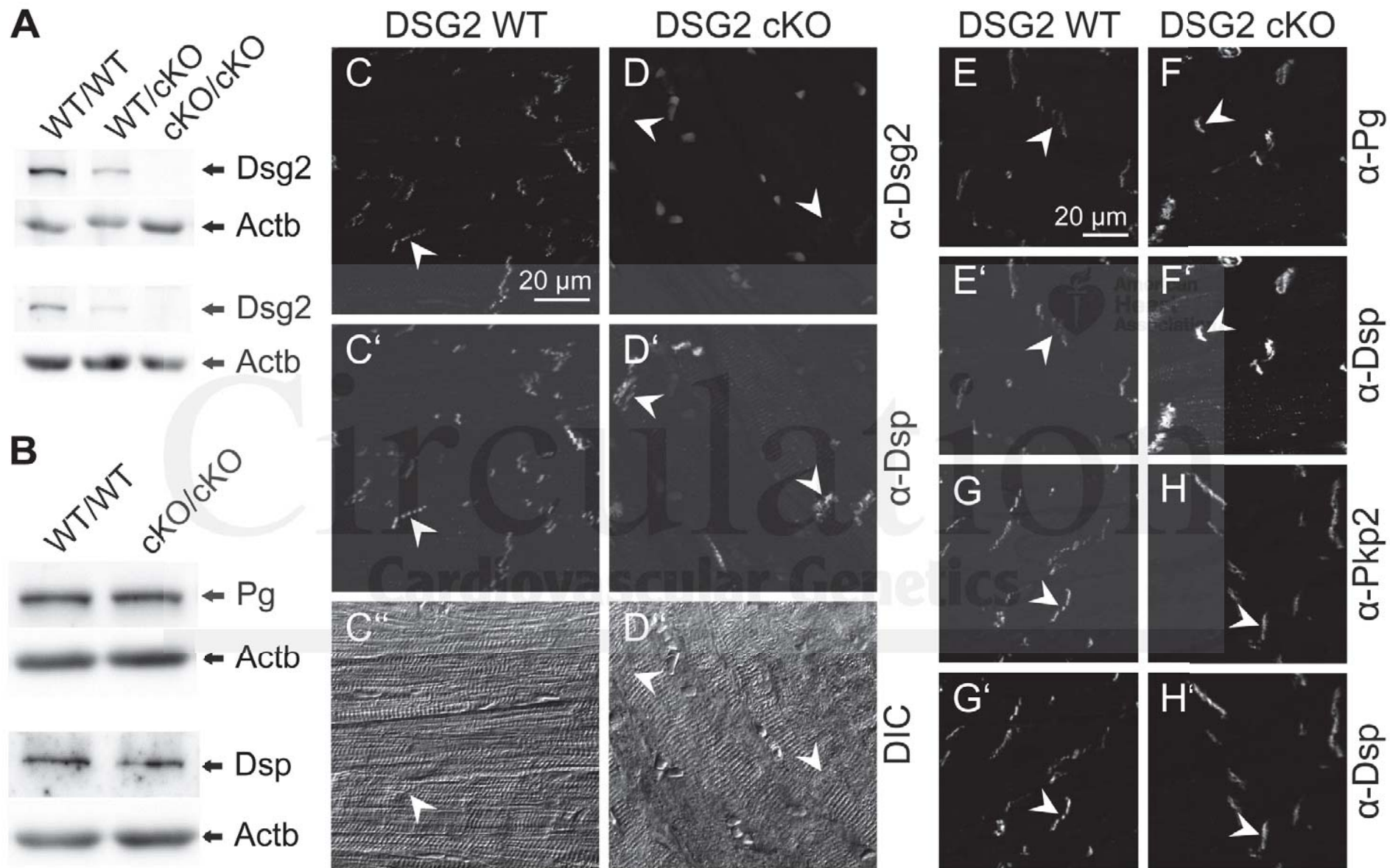
Figure 6: Ultrastructural comparison of $DSG2^{WT}$, $DSG2^{MT}$ and $DSG2^{cKO}$ hearts. (**A-C'**) Electron micrographs of longitudinal sections showing sarcomeres next to IDs. Wild type IDs contain typical desmosome-like structures (arrows), which are not seen in $DSG2^{MT}$ or $DSG2^{cKO}$ mice. In addition, dissociated IDs are frequent in mutant animals (**D-F**). The enlarged intercellular gap is

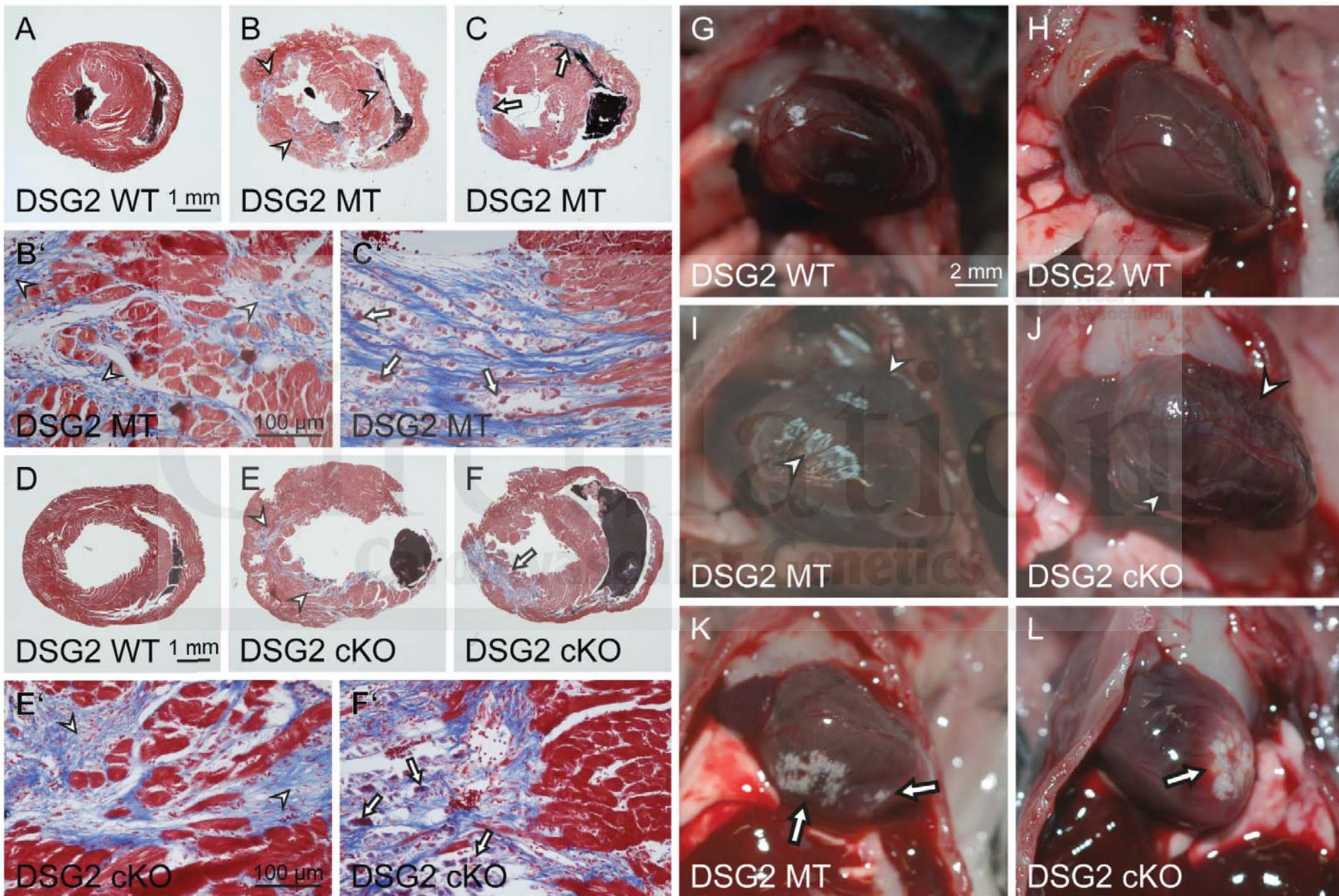
filled with multilamellar bodies (arrowheads) and other cellular organelles such as mitochondria (Mi; **E**). The remains of adhesion structures are still seen as dark accumulations at the borders of the disrupted myocytes (asterisks). (**F-G**) depict cardiomyocytes with normal mitochondria and sarcomeres (Sa) which are located next to collagen-rich fibrotic lesions (Co) and disrupted IDs. Scale bars: 1000 nm in **A, D, F** (same magnifications in each row); 200 nm in **A', B', C'**.

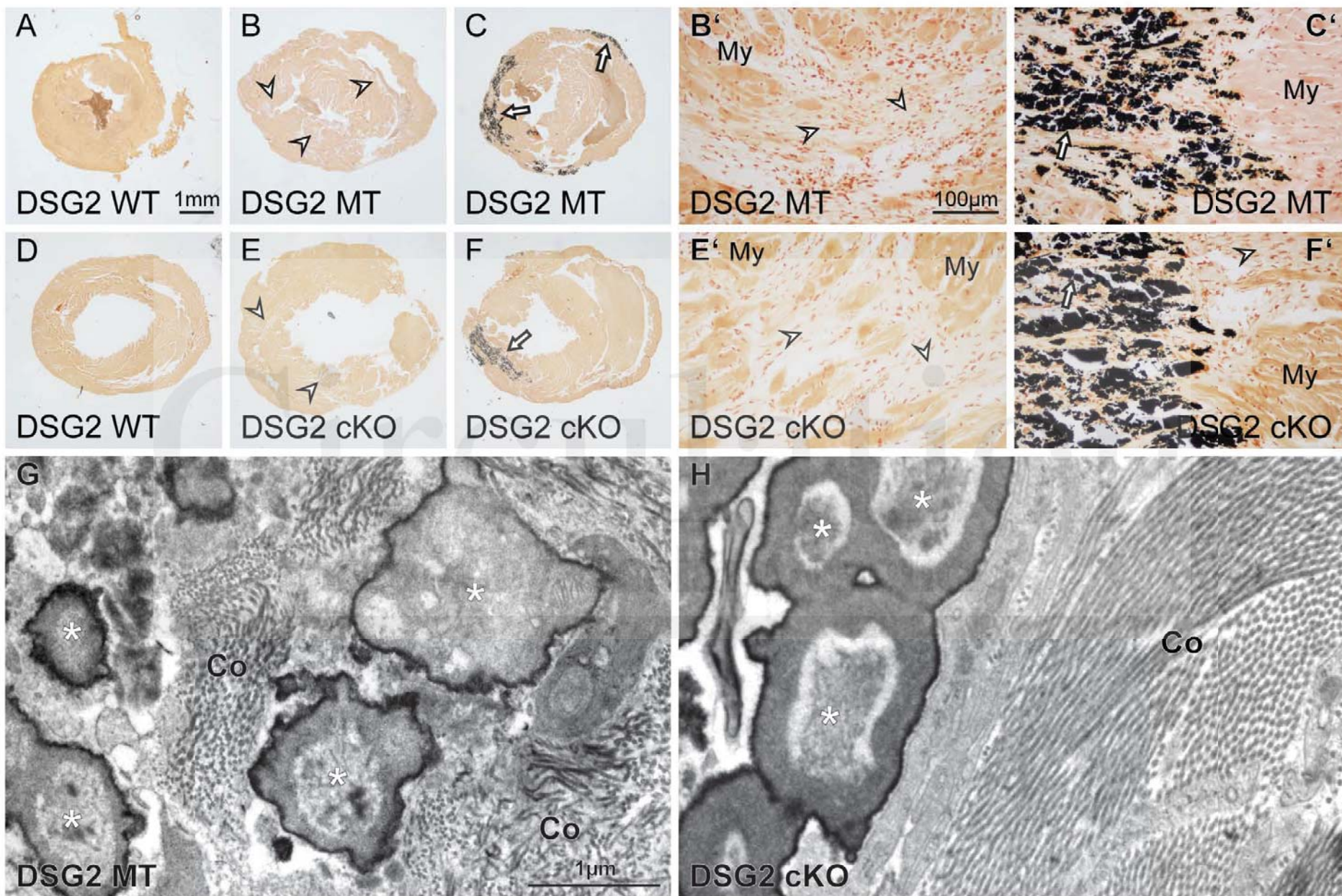
Figure 7: Comparison of connexin 43 expression and electrocardiography of $DSG2^{WT}$, $DSG2^{MT}$ and $DSG2^{cKO}$ mice. (**A-C**) Overlay of anti-connexin 43 immunofluorescence and interference contrast images of 12 week-old mice (n=6 for each genotype) demonstrating typical ID staining in all samples (arrowheads) and prominent cytoplasmic puncta (arrows) in cardiomyocytes next to fibrotic regions (fib) in $DSG2^{MT}$ and $DSG2^{cKO}$ samples. Bar: 50 μm in **C** (same magnification in **A, B**). (**D**) Immunoblot detection of connexin 43 (Cx43) and actin (corresponding Ponceau-staining of PVDF membranes below) in total heart lysates (M, marker lane; MT, $DSG2^{MT}$; WT, $DSG2^{WT}$; cKO, $DSG2^{cKO}$). (**E**) Typical examples of averaged ECGenie recordings of ~20 week-old mice that were used for further analysis. (**F**) Histogram depicting RR, PR and QRS intervals determined in wild type (WT at left; n=6) versus $DSG2^{MT}$ (MT; n=8) and $DSG2^{\text{fllox}(E4-5)}$ (WT at right; n=10) versus $DSG2^{cKO}$ (cKO; n=8) animals. Note the significant increase in PR and QRS intervals in both instances (**p<0.01; ***p<0.001).

Figure 8: Schematic representation of ID-localized desmosomal cadherins and associated signaling molecules in different mouse models with altered *Dsg2* expression. The table also lists, whether overt AC develops until the 12th week after birth. References are given for each animal model.

A**B****C****D**







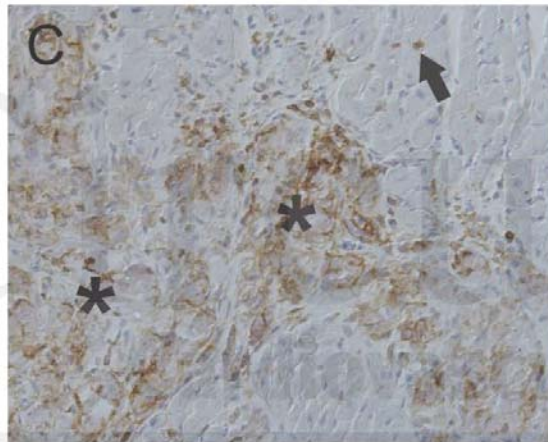
4 weeks

12 weeks

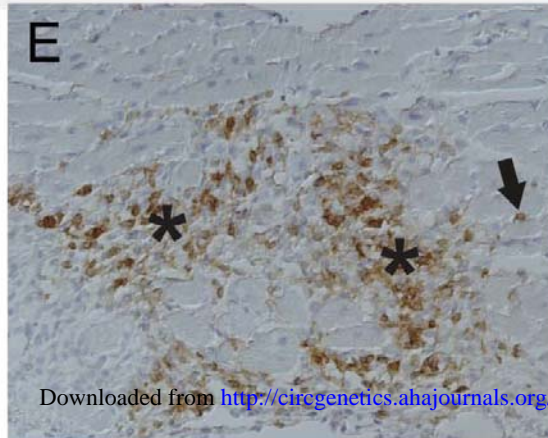
DSG2 WT



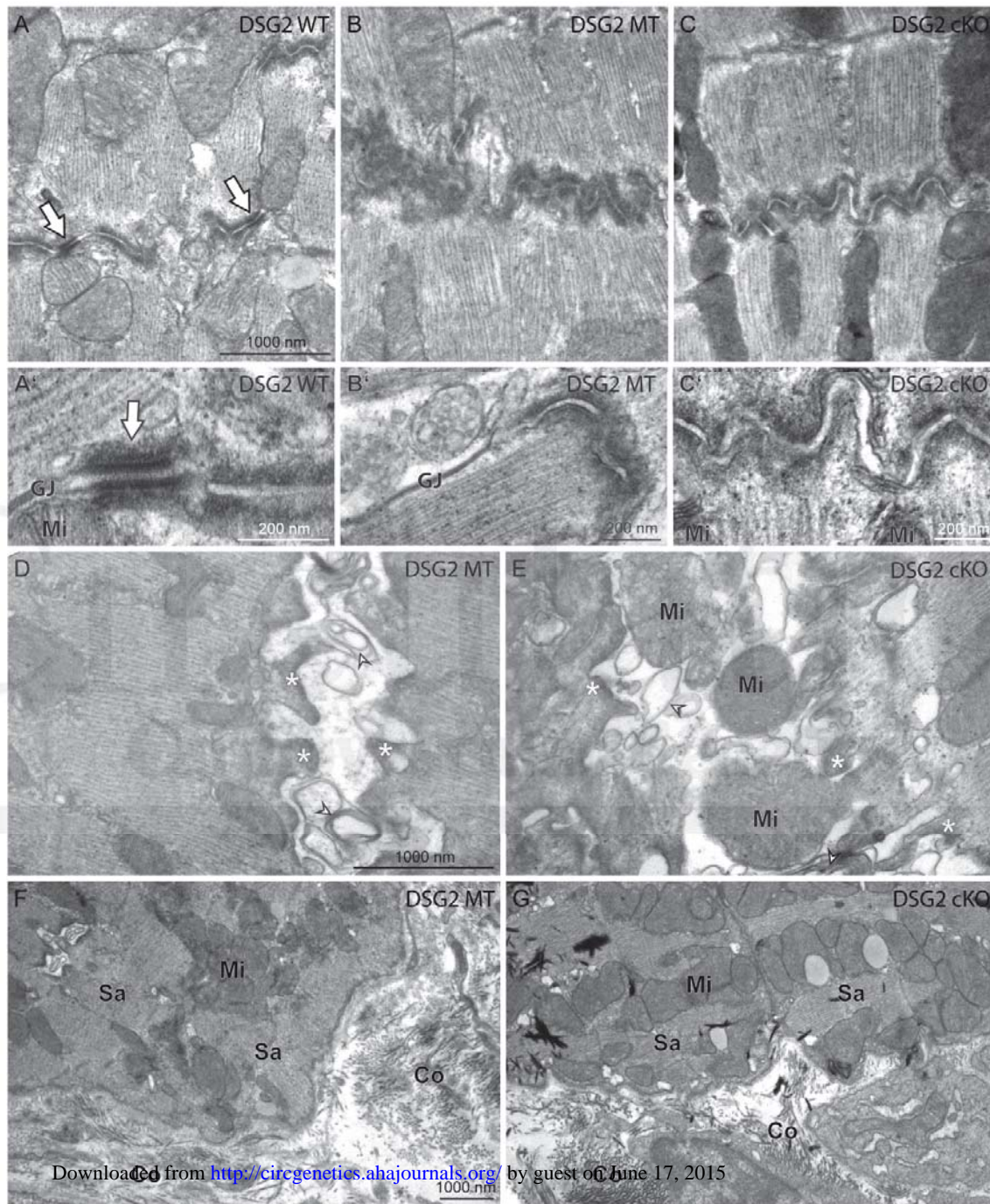
DSG2 MT



DSG2 cKO

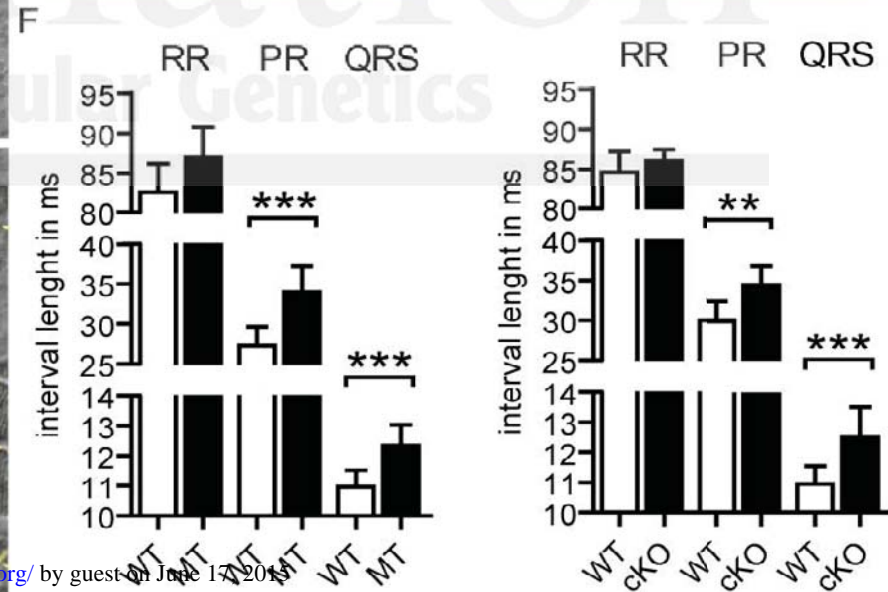
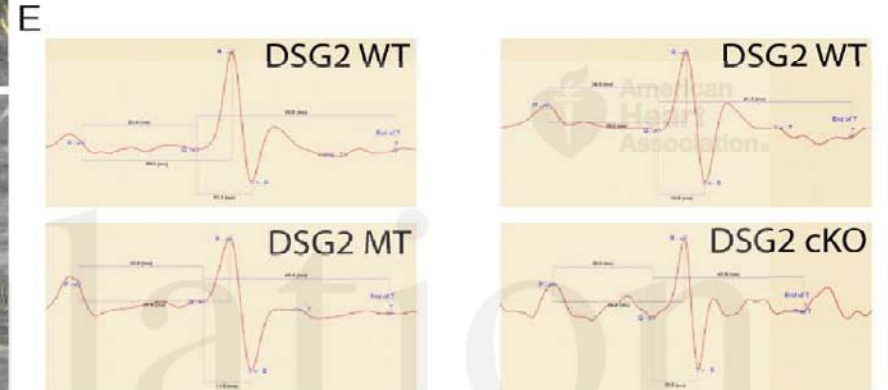
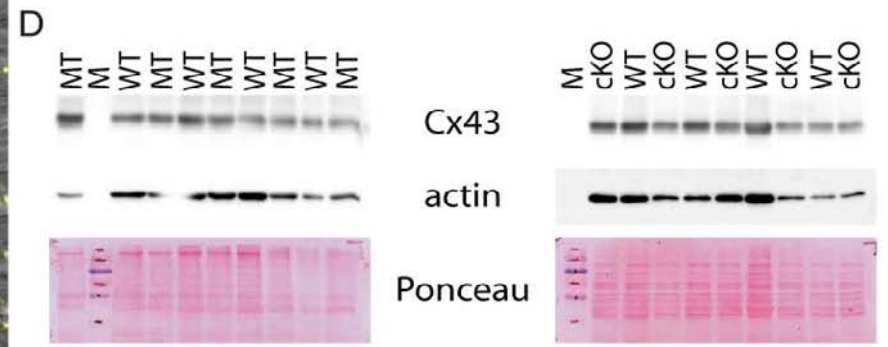
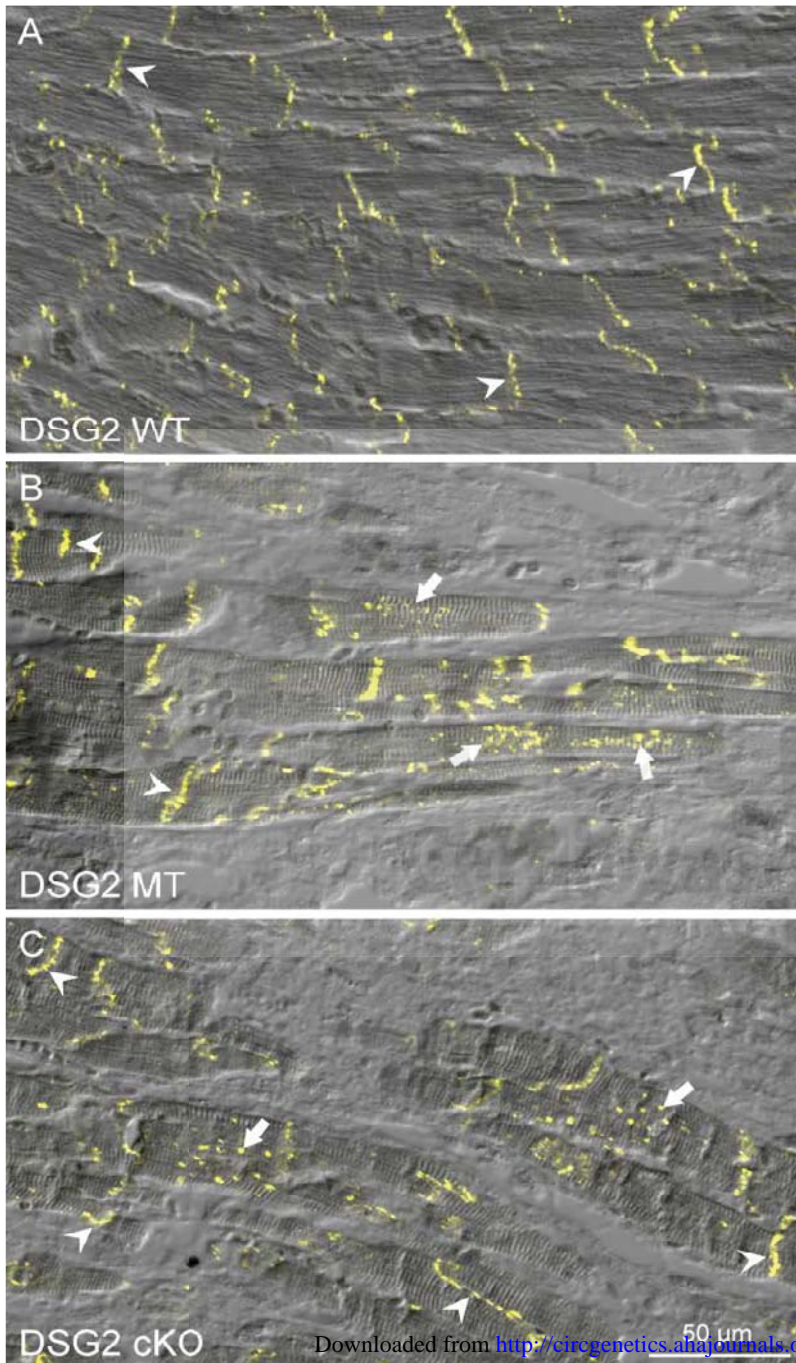


American
Heart
Association



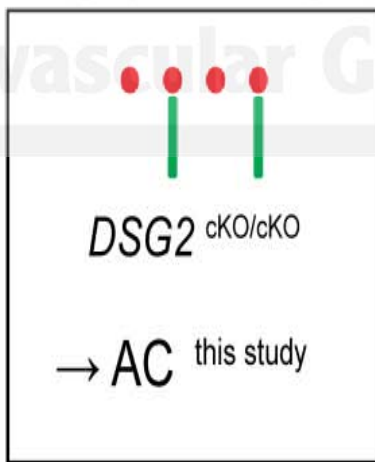
American Heart Association.

n



Genotype	AC		AC	Genotype
$DSG2^{WT/KO}$ ²¹	no			$DSG2^{MT/MT}$ ^{22, 23}
$DSG2^{WT/WT}$	no			$DSG2^{WT/MT}$ ²³
$DSG2^{WT/WT} + tg(WT)$ ¹⁴	no			$DSG2^{WT/WT} + tg(N271S)$ ¹⁴

- plakoglobin/signaling molecule
- desmocollin 2
- desmoglein 2
- adhesion-deficient desmoglein 2



SUPPLEMENTAL MATERIAL

Supplemental Methods

Cloning of targeting construct

To prepare the targeting construct, the *DSG2* 3'-homology region was isolated from clone 3011¹ together with a neomycin resistance (NFL) cassette and the vector backbone as a 9046 bp *XhoI*-fragment and re-ligated resulting in clone 3060. The 2034 bp NFL-cassette was subsequently removed by *EcoRI*-restriction and re-ligation (clone 3062). To clone the 5'-homology region, the *SpeI*-restriction site of pBluescript KS (+) was removed by blunt end formation and re-ligation of *SpeI*-digested vector (clone 3061). The 5569 bp *XhoI* 5'-homology region was then excised from clone 3011 and inserted into clone 3061 resulting in clone 3063.7. The phosphoglycerate kinase-driven neomycin resistance cassette, which is flanked by two FRT-sites and flanked by a single loxP-site at its 3'-end, was amplified from clone 3060 with primers 07-24 (5'-GCC ACT AGT GCT GCG ATT ATA GGC CTG AG-3') / 07-25 (5'-GAT CAC TAG TGC GGG GAT AAT ACG ACT C-3') and was inserted blunt into the *SpeI*-linearized clone 3063.7 (clone 3064.1). Then, the 5'-homology region together with the NFL cassette was isolated as a 7620 bp *XhoI*-fragment from clone 3064.1 and the 7012 bp 3'-homology-vector fragment was isolated by linearization of clone 3062 with *XhoI*. Both fragments were then combined to yield targeting construct 3065.

Generation of knockout mice

Trypsinized AB2.2 embryonic stem (ES) cells (ATCC SCRC-1023) that had been grown in a 10 cm Petri dish were mixed with 200 µg of *NotI*-linearized targeting construct (clone 3065) for electroporation (800 V; 3 µF; 0.04 ms). Electroporated cells were seeded in ES-cell medium (GMEM [Gibco] supplemented with sodium pyruvate [PAA], non-essential amino acids [PAA], 5% fetal calf serum [Invitrogen], 5% newborn calf serum [Gibco], 0.1 mM β-mercaptoethanol, leukemia inhibitory factor [LIF] obtained from supernatants of LIF-expressing COS7 cells) and selected with 350 µg/ml G418 (Gibco). After 10 days G418-resistant clones were isolated and amplified. Genomic DNA was prepared and tested for homologous recombination by PCR to detect the recombined 2355 bp fragment with primers 08-21 (5'-TTT CAG ATT GGT TTA GTG GG-3') and 08-22 (5'-TAT GCT ATA CGA AGT TAT GAT ATC C-3'). PCR-positive ES-cell clones were further examined by Southern blot analysis. ES cell clones with correct *DSG2* recombination were injected into blastocysts or morulae, which were implanted into pseudopregnant foster mothers. The resulting chimeras were bred with C57BL/6J mice and offspring with brown fur was analyzed for recombination by PCR. The transgenic animals were then bred with FLP^o deleter mice (friendly gift from Dr. Anastassiadis, Dresden University)² to remove the neomycin resistance cassette. To obtain cardiomyocyte-specific *DSG2* recombination, mice were bred with αMyHC-Cre (now referred to as Myh6-Cre) transgenic mice (kindly provided by Dr. Schneider, Imperial College London).³

Southern blotting and PCR analyses

25 µg genomic DNA were digested with *EcoRV* and separated on a 0.7% agarose gel. DNA was depurinated in the gel by incubation in 0.25 M HCl for 20 min and was subsequently denatured by treatment with 0.4 M NaOH. DNA was blotted onto a neutral nylon membrane (Hybond-N, GE Healthcare) overnight in 0.4 M NaOH and the membrane was dried for 1 h at 80°C. 200 ng of each probe were labeled using Ladderman Labeling Kit (TaKaRa) according to the instructions of the manufacturer. Easytides dCTP [α -³²P] (Perkin Elmer) were used for probe labeling and labeled probes were purified using Probe Quant G50 Micro Columns (GE Healthcare).

Using primers 10-110 (5'-TCA AGC TTT AGC ACA AAC CAC CCA TGT C-3') and 10-111 (5'-TAG AAT TCG CAC ATT CAT GTG GGA AAC C-3') a 769 bp fragment was amplified from clone 3065 as 5'-probe and cloned into pUC18 after digestion with *EcoRI* and *HindIII* (clone 3067). To prepare a 3'-probe, a 1020 bp fragment was PCR-amplified with the help of primers 10-114 (5'-TAT CTA GAC ATT GAG CCA TCT CCT CAA C -3') and 10-115 (5'-ATG AGC TCA TGT GTC ACC AGG GAT AGT C-3') and inserted after *SacI*/*XbaI*-restriction into pUC18 (clone 3069). Labeled probes were prepared from purified plasmid inserts. Membrane with blotted genomic DNA was rehydrated and blocked at 64°C for 15 min in hybridization buffer (0.5 M phosphate buffer, 3.5% sodium dodecyl sulfate (SDS), pH 7.0, 100 µg/ml denatured salmon sperm DNA). 200 ng of denatured and labeled probe were added and hybridization was performed over night at 64°C. Membrane was shortly washed with wash buffer I (2x SSC [0.33 M NaCl and 30 mM trisodium citrate, adjusted to pH 7.0 with HCl], 0.1% SDS) at room temperature, followed by two washings for 20 min with wash buffer II (1x SSC, 0.1% SDS) at 64°C. Finally, the membrane was washed for 30 min with wash buffer III (0.1x SSC, 0.1% SDS) at room temperature.

A 406 bp internal probe was amplified from the targeting construct using primers 03-63 (5'-TCA GCA GAC TCG GCA ACA AG-3') and 03-69 (5'-AAT CGA GGG AGT GGA GAA AC-3'). In this instance, the membrane-blotted DNA was rehydrated with Church buffer (40 mM phosphate buffer, 1% SDS, pH 6.8) at 65°C for 15 min. Blocking of unspecific probe hybridization was achieved by membrane incubation with pre-warmed QuikHyb Hybridisation Solution (Stratagene) containing 100 µg/ml denatured salmon sperm DNA. 200 ng of denatured and labeled probe were added and hybridization was performed over night at 65°C. Afterwards, membrane was washed 3 times with Church buffer at 62°C for 20 min.

Hybridization of probes was detected with the help of BioMax MR Film (Kodak) by autoradiography.

To determine whether Myh6-Cre driven recombination was successful a PCR using genomic DNA obtained from heart tissue and primers 12-7 (5'-GGT AAA TGC AGA CGG ATC AG-3'), 12-8 (5'-TGG GCT ACA CTC ATA GGA AG-3') and 12-99 (5'-TTG CAC AGG ACT CAG GAT TG-3') was performed.

RNA isolation, reverse transcription and qRT-PCR

Fresh tissue samples were homogenized in extraction buffer (PeqlabGold RNA kit, Peqlab) and proteins were removed using phenol/chloroform precipitation. Total RNA was then enriched using the PeqlabGold RNA kit in combination with on column DNase digestion according the instruction manual of the manufacturer (Peqlab).

To prepare cDNA, mRNA was reverse-transcribed using the Transcriptor First Strand cDNA Synthesis kit with oligo-(dT)₁₈ oligonucleotides (Roche). qRT-PCR was performed with a LightCycler 96 (Roche), FastStart Essential DNA Green Master Kit or FastStart Essential DNA Probes Master (Roche) and the following forward, reverse primers and UPL-probes (Roche): wild type-specific *DSG 2* (13-78 forward 5'-ACC GGG AAG AAA CAC CAT ATT-3'; 13-79 reverse 5'-AGG GCT TTT CCA GGT TGT TT-3'), *ANF* (09-50 forward 5'-CAC AGA TCT GAT GGA TTT CAA GA-3'; 09-51 reverse 5'-CCT CAT CTT CTA CCG GCA TC-3'; UPL-probe 25), *CTGF* (09-20 forward 5'-TGA CCT GGA GGA AAA CAT TAA GA-3'; 09-21 reverse 5'-TGA CCT GGA GGA AAA CAT TAA GA-3'; UPL-probe 71), *GDF15* (09-78 forward 5'-GAG CTA CGG GGT CGC TTC-3'; 09-79 reverse 5'-GGG ACC CCA ATC TCA CCT-3'; UPL-probe 62), *HMBS* housekeeping control (12-36 forward 5'-AAG TTC CCC CAC CTG GAA-3'; 12-37 reverse 5'-GAC GAT GGC ACT GAA TTC CT-3'; UPL-probe 42), *HPRT* housekeeping control (12-65 forward 5'-TGA TAG ATC CAT TCC TAT GAC TGT AGA-3'; 12-66 reverse 5'-AAG ACA TTC TTT CCA GTT AAA GTT GAG-3') and *TBP* housekeeping control (11-25 forward 5'-GGG GAG CTG TGA TGT GAA GT-3'; 11-26 reverse 5'-CCA GGA AAT AAT TCT GGC TCA-3').

Generation of polyclonal Dsg2 antibody

The antigen was obtained by conjugation of the synthetic peptide with sequence SVTKGQHELSEVDGRWEEHRSC to ovalbumine. The antibodies were generated in guinea pig by subcutaneous injection of 240 µg immunogenic polypeptide diluted in complete Freund's adjuvant followed by three boosting injections with 240 µg antigen diluted in incomplete Freund's adjuvant every two weeks. Serum was collected 14 days after the last immunization.

Immunoblotting

Fresh tissue samples were Dounce-homogenized in extraction buffer (10 mM Tris-HCl [pH 8.0], 2 mM MgCl₂, 10 mM KCl, 2% SDS supplemented with a complete mini protease inhibitor tablet per 10 ml [Roche]) and stored on ice. After preparation of all samples, they were heated at 94°C for 10 min and then directly placed on ice for 5 min. Lysates were cleared by centrifugation (4°C, 17000 g, 20 min) to obtain whole heart protein extract in the supernatant. Protein concentration was determined using DC Protein Assay (BioRad). 35 µg of protein per lane were separated by SDS-polyacrylamide gel electrophoresis and transferred onto polyvinylidene fluoride (PVDF) membranes using tank-blotting. Membranes were afterwards blocked with 5% (w/v) low fat milk powder (Roth) in TBST (50 mM Tris-HCl [pH 7.6], 150 mM NaCl, 0.1% (v/v) Tween 20) for 2 h, washed 3 times for 5 min each with TBST and incubated with primary antibody diluted in TBST/1% low fat milk powder overnight at 4°C. Antibody dilutions were: 1:2500 for polyclonal rabbit anti-Dsg2 antibodies (Dsg2 IC)⁴ and polyclonal guinea pig anti-Dsg2 antibodies (see previous paragraph), 1:1000 goat anti-Pg (sc-30997, Santa Cruz), 1:200 mouse anti-Dsp (65146, Progen), 1:4000 rabbit anti Cx43 (C6219, Sigma), 1:4000 for polyclonal rabbit anti β-actin antibodies (A2066, Sigma). Membranes were washed 3 times in TBST and incubated for 1 h with horseradish peroxidase-coupled secondary antibodies (anti-rabbit and anti-goat antibodies from DAKO at 1:5000 and anti-guinea pig antibodies from Jackson at 1:5000, both diluted in TBST with 1% low fat milk powder). Signals were detected using ECL prime (GE healthcare) and a chemiluminescence imaging system (Fusion SL, Vilber Lourmat).

Supplemental Figures

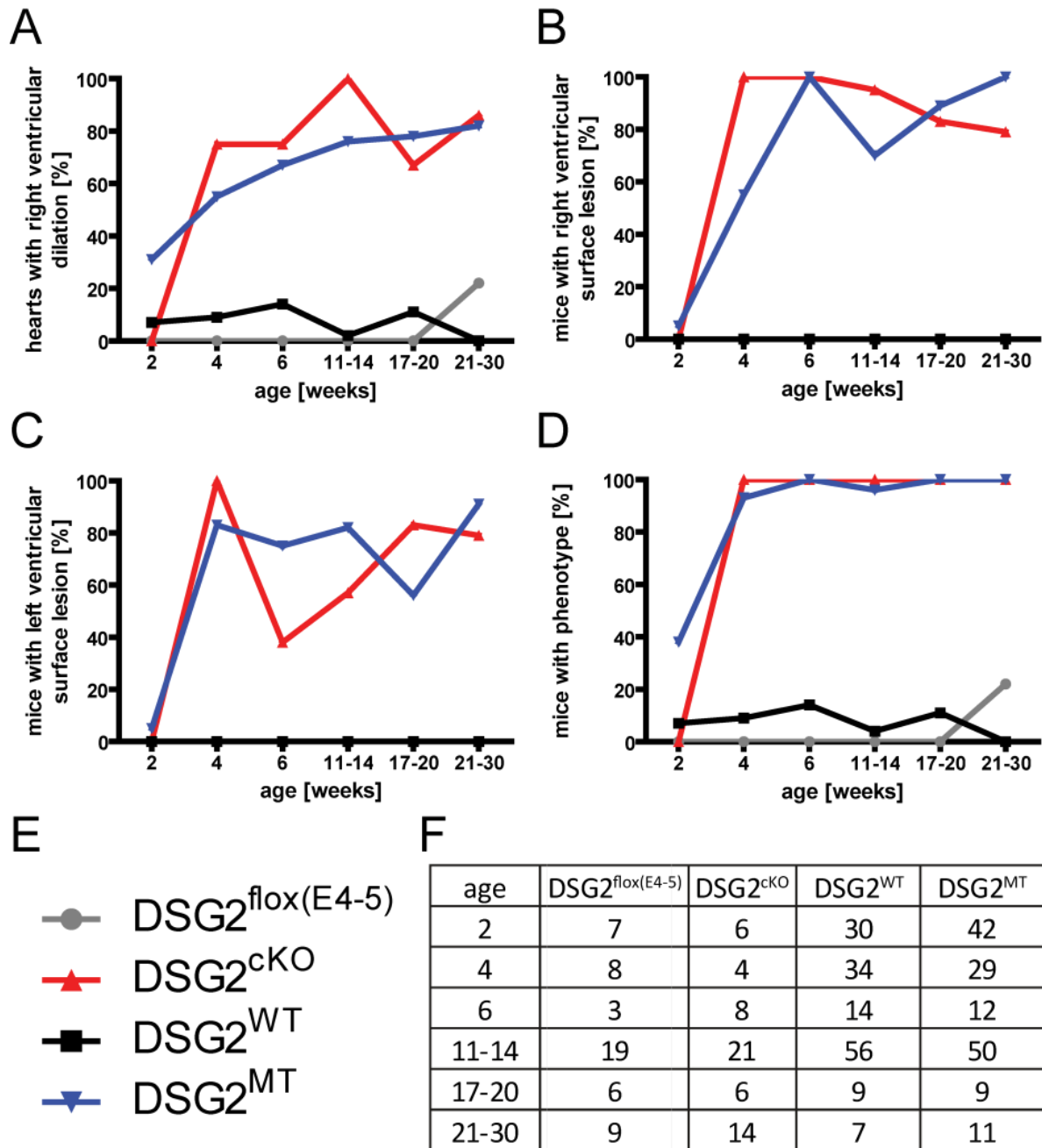


Figure S1. Gross morphological evaluation of dissected hearts taken from homozygous $DSG2^{MT}$ and $DSG2^{cKO}$ mice and $DSG2^{WT}$ or $DSG2^{flox(E4-5)}$ control animals. The graphs show the percentage of animals presenting dilation of the right ventricle (A) or visible surface lesions on the right (B) or left ventricle (C). The summary graph in (D) shows the percentage of animals with at least one phenotypic deviation. Note, that by 4 weeks 93% of the $DSG2^{MT}$ and 100% of the $DSG2^{cKO}$ mutant hearts are visibly abnormal. (E) represents the legend for A-D and (F) a listing of the number of animals examined for each phenotype at each time point.

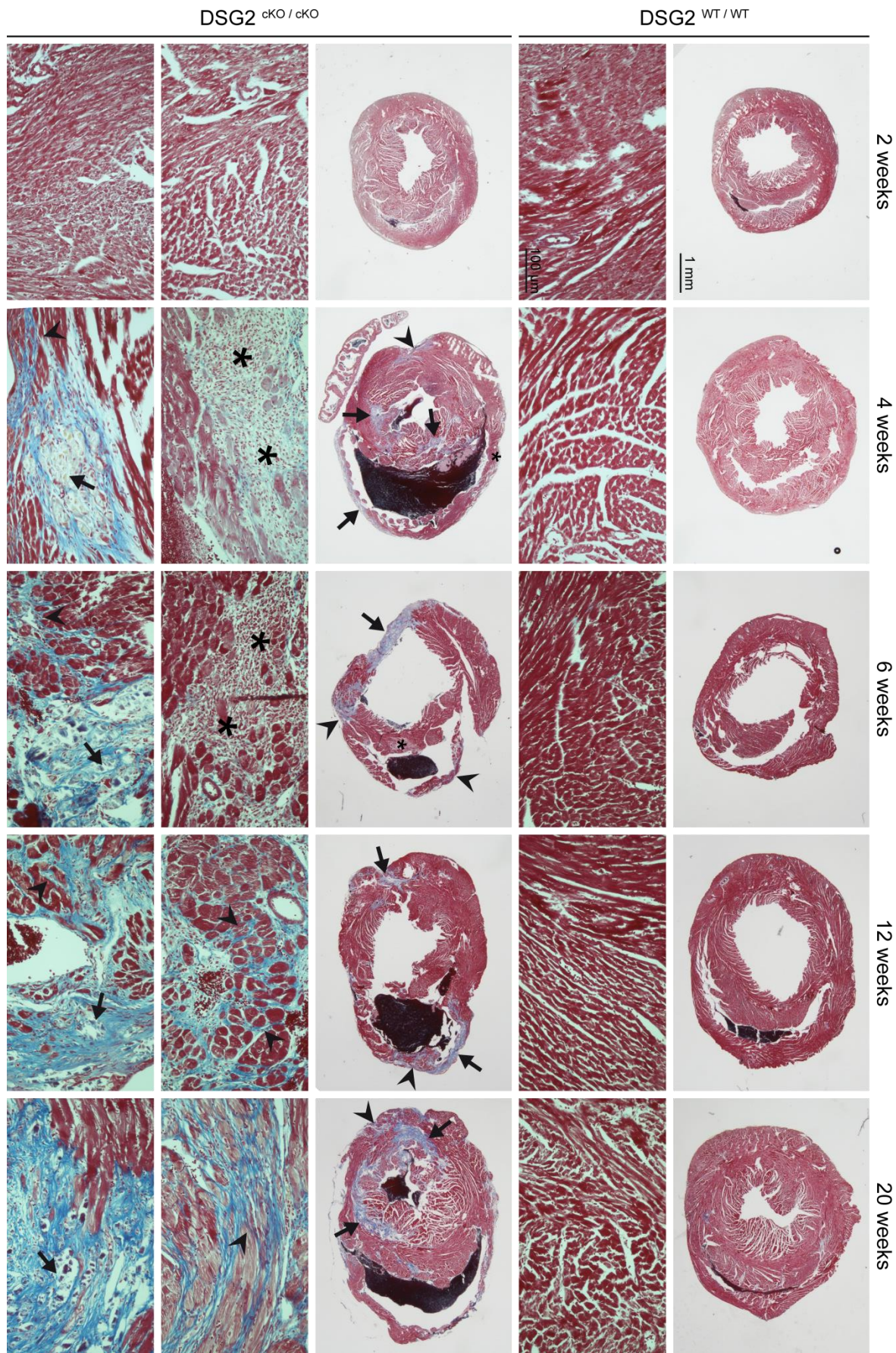


Figure S2. Photomicrographs of Azan-stained myocardial sections obtained from *DSG2*^{WT} and *DSG2*^{cko} animals highlighting the disease stages. Note the normal-appearing myocardium at 2 weeks and the formation of immune cell-rich lesions (*) in areas of cardiomyocyte death at 4 weeks (arrows) forming collagen-rich fibrotic foci. In addition, interstitial fibrosis increases over time (arrowheads). Scale bar: 1 mm for all survey views; 100 μ m for all higher magnifications.

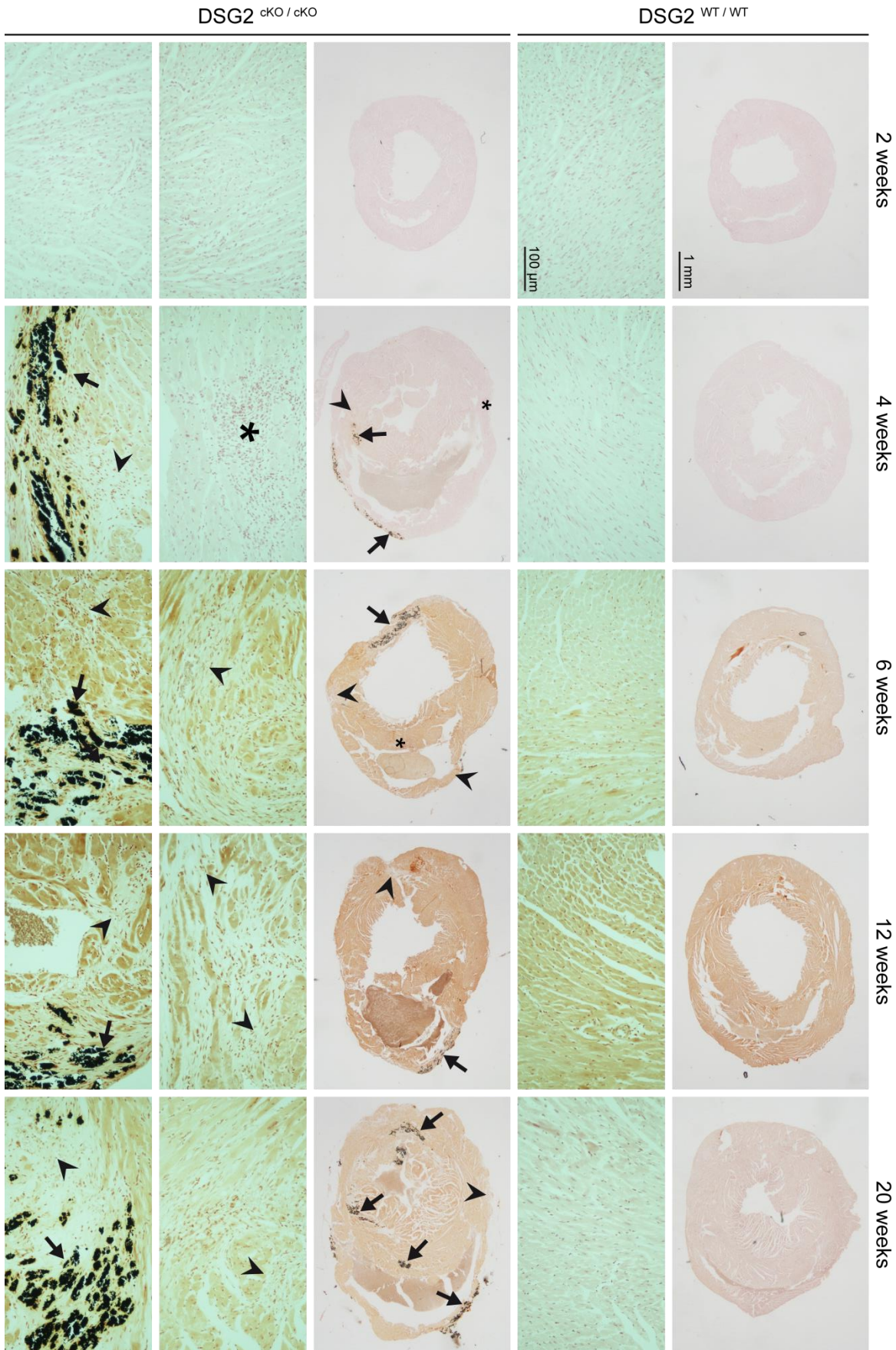


Figure S3. Pictures of von Kossa-stained myocardial sections obtained from *DSG2*^{WT} and *DSG2*^{ckO} animals depicting calcium deposition in lesions of mutant hearts. Note that the fibrotic lesions (arrows) present prominent black precipitates that are not yet detectable in fresh immune cell-rich lesions (*) and regions with interstitial fibrosis (arrowheads). Scale bar: 1 mm for all survey views; 100 μ m for all higher magnifications.

References

1. Krusche CA, Holthofer B, Hofe V, van de Sandt AM, Eshkind L, Bockamp E, et al. Desmoglein 2 mutant mice develop cardiac fibrosis and dilation. *Basic Res Cardiol*. 2011;106:617-633.
2. Kranz A, Fu J, Duerschke K, Weidlich S, Naumann R, Stewart AF, et al. An improved flp deleter mouse in c57bl/6 based on flpo recombinase. *Genesis*. 2010;48:512-520.
3. Agah R, Frenkel PA, French BA, Michael LH, Overbeek PA, Schneider MD. Gene recombination in postmitotic cells. Targeted expression of cre recombinase provokes cardiac-restricted, site-specific rearrangement in adult ventricular muscle in vivo. *J Clin Invest*. 1997;100:169-179.
4. Schlegel N, Meir M, Heupel WM, Holthofer B, Leube RE, Waschke J. Desmoglein 2-mediated adhesion is required for intestinal epithelial barrier integrity. *Am J Physiol Gastrointest Liver Physiol*. 2010;298:G774-783.

Desmoglein 2-Dependent Arrhythmogenic Cardiomyopathy Is Caused by a Loss of Adhesive Function

Sebastian Kant, Bastian Holthöfer, Thomas M. Magin, Claudia A. Krusche and Rudolf E. Leube

Circ Cardiovasc Genet. published online June 17, 2015;

Circulation: Cardiovascular Genetics is published by the American Heart Association, 7272 Greenville Avenue, Dallas, TX 75231

Copyright © 2015 American Heart Association, Inc. All rights reserved.

Print ISSN: 1942-325X. Online ISSN: 1942-3268

The online version of this article, along with updated information and services, is located on the World Wide Web at:

<http://circgenetics.ahajournals.org/content/early/2015/06/17/CIRCGENETICS.114.000974>

Data Supplement (unedited) at:

<http://circgenetics.ahajournals.org/content/suppl/2015/06/17/CIRCGENETICS.114.000974.DC1.html>

Permissions: Requests for permissions to reproduce figures, tables, or portions of articles originally published in *Circulation: Cardiovascular Genetics* can be obtained via RightsLink, a service of the Copyright Clearance Center, not the Editorial Office. Once the online version of the published article for which permission is being requested is located, click Request Permissions in the middle column of the Web page under Services. Further information about this process is available in the [Permissions and Rights Question and Answer](#) document.

Reprints: Information about reprints can be found online at:
<http://www.lww.com/reprints>

Subscriptions: Information about subscribing to *Circulation: Cardiovascular Genetics* is online at:
<http://circgenetics.ahajournals.org/subscriptions/>